

Dalton Transactions

Accepted Manuscript



This is an *Accepted Manuscript*, which has been through the Royal Society of Chemistry peer review process and has been accepted for publication.

Accepted Manuscripts are published online shortly after acceptance, before technical editing, formatting and proof reading. Using this free service, authors can make their results available to the community, in citable form, before we publish the edited article. We will replace this *Accepted Manuscript* with the edited and formatted *Advance Article* as soon as it is available.

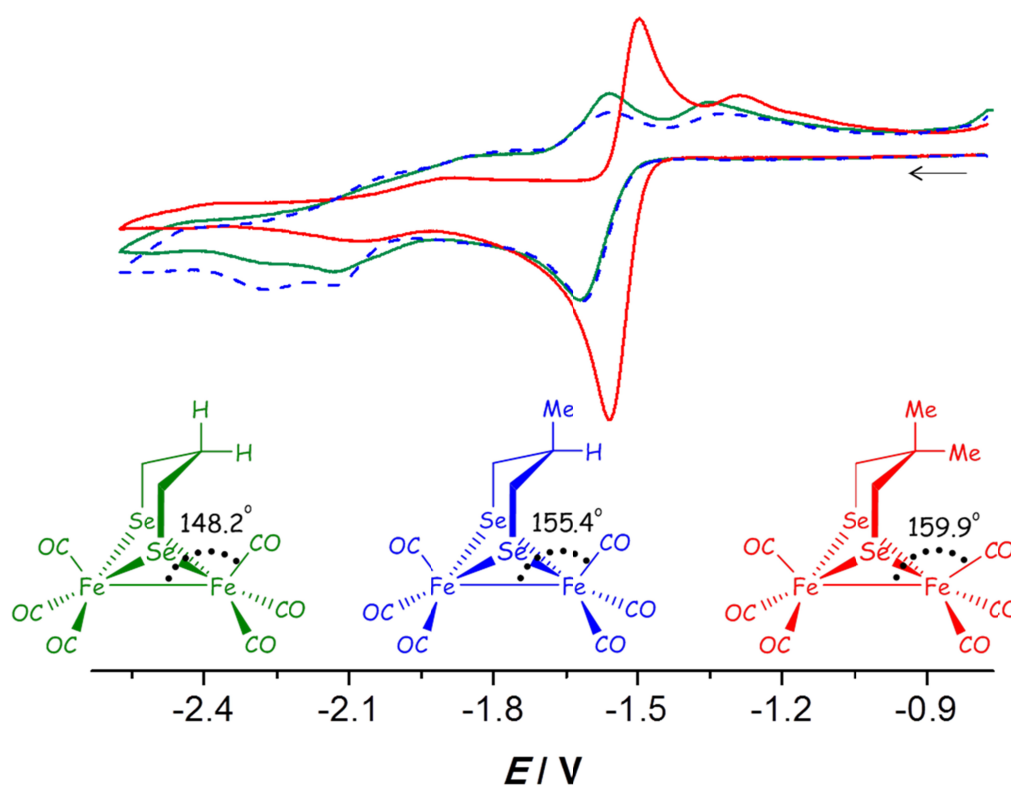
You can find more information about *Accepted Manuscripts* in the [Information for Authors](#).

Please note that technical editing may introduce minor changes to the text and/or graphics, which may alter content. The journal's standard [Terms & Conditions](#) and the [Ethical guidelines](#) still apply. In no event shall the Royal Society of Chemistry be held responsible for any errors or omissions in this *Accepted Manuscript* or any consequences arising from the use of any information it contains.

***Steric Effect of the Dithiolato Linker on the
Reduction Mechanism of $[Fe_2(CO)_6\{\mu-(XCH_2)_2CRR'\}]$ Hydrogenase Models ($X = S, Se$)***

Laith R. Almazahreh,[‡] Ralf Trautwein,[‡] Helmar Görls and Wolfgang Weigand*

[‡] Equal contributors



***Steric Effect of the Dithiolato Linker on the Reduction
Mechanism of $[Fe_2(CO)_6\{\mu-(XCH_2)_2CRR'\}]$
Hydrogenase Models ($X = S, Se$)***

Laith R. Almazahreh,^{a,‡} Ralf Trautwein,^{a,‡} Helmar Görls^a and Wolfgang Weigand^{a,b,}*

*^aInstitut für Anorganische und Analytische Chemie, Friedrich-Schiller-Universität Jena,
Humboldtstrasse 8, D-07743 Jena, Germany,*

^bJena Center of Soft Matter (JCSM), Philosophenweg 7, D-07743 Jena, Germany

[‡]Equal contributors

AUTHOR EMAIL ADDRESS (wolfgang.weigand@uni-jena.de)

RECEIVED DATE (to be automatically inserted after your manuscript is accepted if required according to the journal that you are submitting your paper to)

* To whom correspondence should be addressed. E-mail: wolfgang.weigand@uni-jena.de (W.W.), Fax: +49 3641 948102, Tel: +49 3641 948160

Abstract:

Studying the redox features of the [FeFe]-hydrogenase models is essential for understanding the function of the H cluster. The reduction of the [FeFe]-hydrogenase models of the type $[\text{Fe}_2(\text{CO})_6\{\mu-(\text{XCH}_2)_2\text{E}\}]$ ($\text{X} = \text{S}, \text{Se}$) is described to occur either via sequential transfer of two electrons at E°_1 and E°_2 for the first and the second reduction steps, respectively, where $E^\circ_1 - E^\circ_2 > 0$, or via transfer of two electrons at the same applied potential due to potential inversion of the two reduction steps, i.e. $E^\circ_1 - E^\circ_2 < 0$. Typically, the phenomenon of potential inversion is observed when a structural change intervenes in the cathodic process stabilizing the reduced species. In this report, we investigate the mechanism of the cathodic process of series of models $[\text{Fe}_2(\text{CO})_6\{\mu-(\text{XCH}_2)_2\text{E}\}]$ ($\text{X} = \text{S}$ or Se and $\text{E} = \text{CH}_2, \text{CHMe}$ or CMe_2) applying cyclic voltammetry. The studies herein show the remarkable influence of the steric bulk of E toward the cathodic process, such that only complexes with $\text{E} = \text{CMe}_2$ are reduced with inverted potentials due to occurrence of an ECE mechanism ($\text{E} = \text{electrochemical process}, \text{C} = \text{chemical process}$) of reduction. Moreover, we describe the catalytic behaviour of these models toward reduction of protons using acetic acid, AcOH , as a proton source.

Keywords: [FeFe]-hydrogenase / Steric effect / Reduction mechanism / Sulfur / Selenium

Introduction

[FeFe]-Hydrogenases are enzymes capable of catalyzing the reversible interconversion of protons and molecular hydrogen with high turnover frequency up to 9000 s^{-1} .¹⁻⁵ The active site of the [FeFe]-hydrogenase contains an organometallic cluster, so called H cluster, which is responsible for the catalytic reduction of protons (Figure 1).^{1,2,6-11} In Figure 1, two redox states of the H cluster are shown, the reduced H_{red} and the oxidized H_{ox} states.^{1,2,6-11} One of the most important structural features of the H cluster, which is responsible for the high catalytic activity, is the presence of a vacant site at one iron core for proton interaction in the H_{red} state or H_2 oxidation in the H_{ox} state.¹⁻¹¹

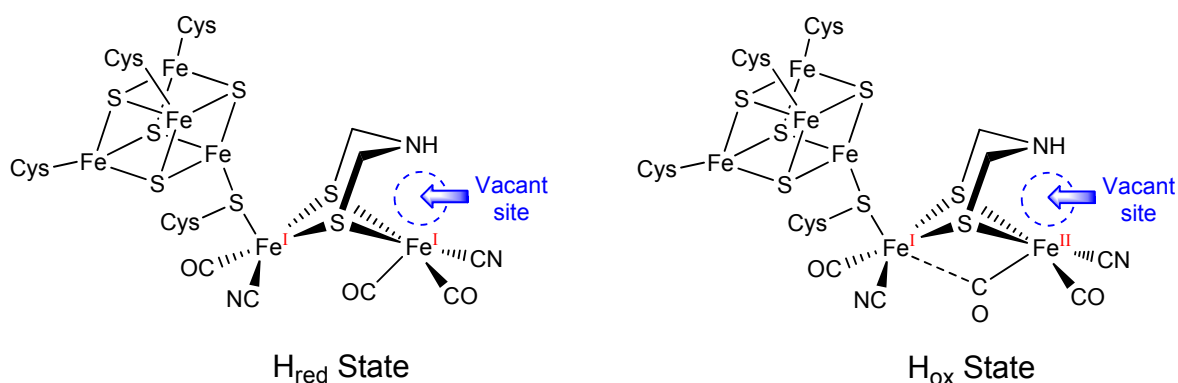


Figure 1. Two redox states of the H cluster of the [FeFe]-hydrogenase: H_{red} and H_{ox} .

In total picture, any successful model catalyst must possess a vacant site or must be able to generate it during the catalytic cycle. Indeed, within the numerous models for the H_{red} in which the two iron units are in a fully/distorted eclipsed conformation,¹²⁻¹⁸ only two models are reported to adopt a rotated structure^{19,20} and one model exhibits a semi-rotated state²¹ (Figure 2). The stabilization of these models in the rotated/semi-rotated states is found to depend on the *steric bulk* of their dithiolato ligands, the desymmetrization of the electron density of the two iron units and the presence of agostic interactions in the case of the models in Figures 2a and b.

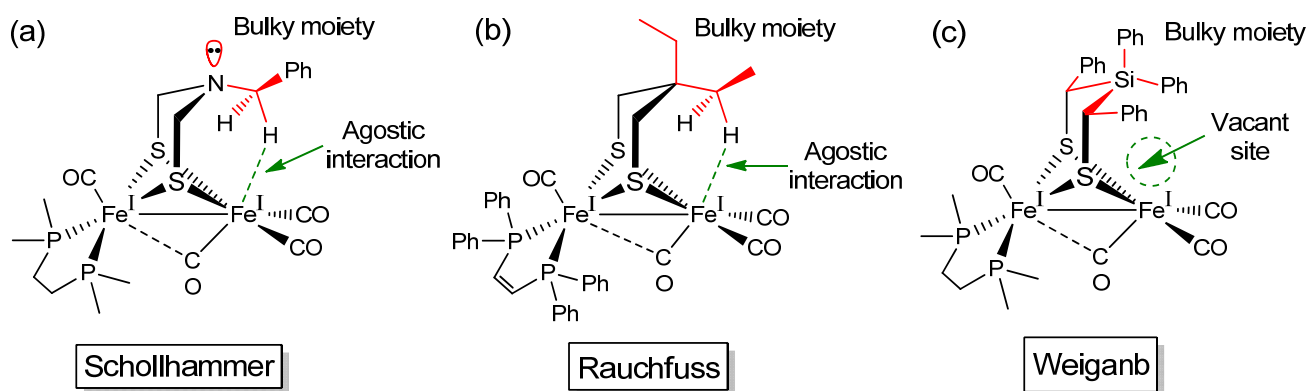


Figure 2. The only models for the H_{red} featuring rotated structures (a¹⁹ and b²⁰) or semi-rotated structure (c)²¹.

For models that do not feature a rotated state at the $[Fe^I Fe^I]$ redox level, it has been described by DFT calculations^{22,23} as well as spectroscopy²³ that a structural change might take place during their

reduction leading to stabilization of one CO ligand in a semi-bridging position to delocalize the negative charge and hence stabilizing the reduced species and resulting in the phenomenon of potential inversion; i.e. $E^{\circ}_1 - E^{\circ}_2 < 0$. Indeed, not all [FeFe]-hydrogenase models undergo an overall two-electron reduction. For example, the models $[\text{Fe}_2(\text{CO})_6\{\mu\text{-(XCH}_2)_2\text{E}\}]$ ($\text{X} = \text{S}$ or Se , $\text{E} = \text{S}$ or Se)²⁴ tend to be reduced with inverted potential whereas in the case of $\text{E} = \text{O}$ ²⁵, the $[\text{Fe}_2\text{S}_2]$ core is reduced with the normal ordering of potentials (i.e. E°_1 is less negative than E°_2). The complex $[\text{Fe}_2(\text{CO})_6\{\mu\text{-bdt}\}]$ (bdt = benzenedithiolato) is reduced by two electrons in a single step due to its ability to stabilize one CO in a semi-bridging position in the monoanion and the dianion.²⁶ The cathodic process of the complexes $[\text{Fe}_2(\text{CO})_6\{\mu\text{-(XCH}_2)_2\text{C}(\text{CH}_2\text{OH})_2\}]$ ($\text{X} = \text{S}$ or Se),²⁷ $[\text{Fe}_2(\text{CO})_6\{\mu\text{-(SCH}_2)_2\text{SiR}_2\}]$ ²³ and $[\text{Fe}_2(\text{CO})_6\{\mu\text{-(SCH}_2)_2(\text{Ph})\text{P=O}\}]$ ²⁸ involves transfer of two-electrons at the same applied potential due to potential inversion. In the case of the model $[\text{Fe}_2(\text{CO})_6\{\mu\text{-(SCH}_2)_2\text{CH}_2\}]$, there is some controversy regarding the overall number of transferred electrons giving rise to the first voltammetric reduction wave, with some claiming two-electrons and others only one.^{22a,24a,29} It has also been described that at rapid scan rates the reduction peak of $[\text{Fe}_2(\text{CO})_6\{\mu\text{-(SCH}_2)_2\text{CH}_2\}]$ splits into two one-electron peaks.^{22a} Clearly, the mechanism of the cathodic process of $[\text{Fe}_2(\text{CO})_6\{\mu\text{-(XCH}_2)_2\text{E}\}]$ is highly dependent on the nature of the $\mu\text{-(XCH}_2)_2\text{E}$ ligand and a well understanding of the thermodynamics and the kinetics of the cathodic processes involved in the cyclic voltammetry of any [FeFe]-hydrogenase model is essential and basic to propose a mechanism for its catalytic behaviour toward reduction of protons. Indeed, the ability of a model complex to stabilize one CO ligand in the semi-bridging position could enhance its catalytic activity toward reduction of protons because the presence of a vacant site may lead to formation of the kinetically labile terminal-hydride species during the turnover. Consequently, it is of great importance to understand the factors that lead to inverted potentials of the two-electron reduction of the model complexes.

In this report, we study in a systematic manner the cathodic process of a series of complexes **1-6** (Figure 3) having the general formula $[\text{Fe}_2(\text{CO})_6\{\mu\text{-(XCH}_2)_2\text{CRR}'\}]$ ($\text{X} = \text{S}$ or Se and R or $\text{R}' = \text{H}$ or Me) by applying cyclic voltammetry. While complexes **1-4** have been already reported,^{24c,30} we herein

synthesize new models **5** and **6** and describe their spectroscopic as well as molecular structural properties in comparison to **1-4**. Our voltammetric investigations of **1-6** reveal that the mechanism of the cathodic process is highly affected by the number of the Me substituents on the bridgehead carbon atom or in other words, the steric bulk of the bridgehead group CRR'. In addition, we herein examine the catalytic properties of **1-6** using AcOH as a proton source.

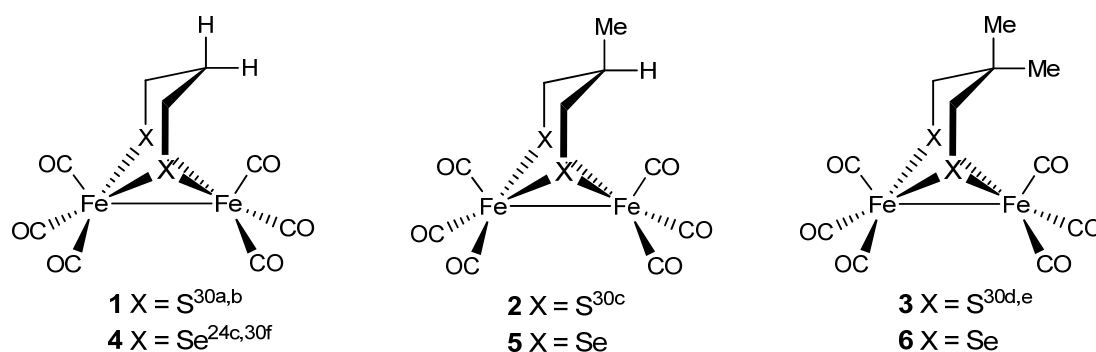
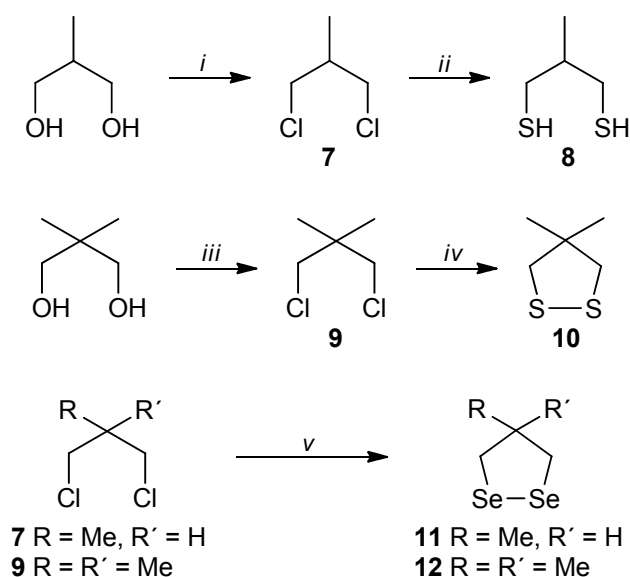


Figure 3. [FeFe]-Hydrogenase models **1-6** used for the electrochemical investigations in this report.

Results and Discussion

Synthesis and characterization of the precursors for the Models 1-6. The synthetic procedures of the precursors **7-12** required for the preparation of complexes **1-6** (see Figure 3) is shown in Scheme 1.³¹ The syntheses of compounds **8**, **10** and **12** were done by modification of the literature methods whereas the new 1,2-diselenolane compound **11** was synthesized in 47 % yield by a similar route as described for the symmetrically substituted diselenolane **12** starting from **7** and **9**.

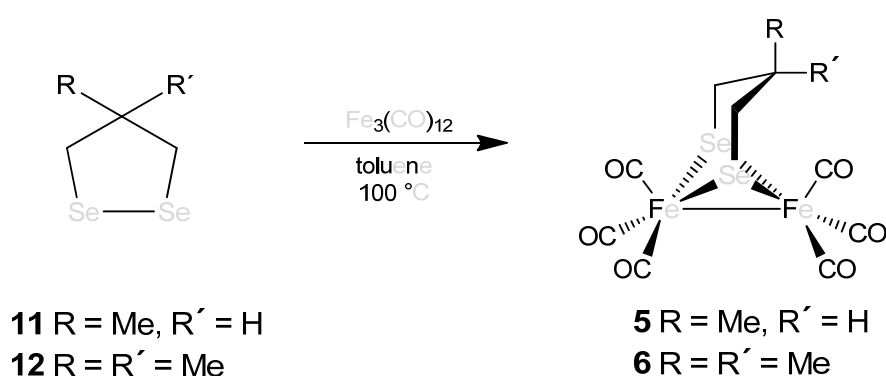
Scheme 1. Synthesis of compounds **8**, **10**, **11** and **12**. *i*) SOCl_2 , PPh_3 , $80\text{-}130^\circ\text{C}$, 7 h;^{31a,h} *ii*) 1. $\text{Na}_2\text{S}\cdot 9\text{H}_2\text{O}$, S, DMF, 130°C , 16 h; 2. NaBH_4 , EtOH, r.t., 3 h;^{31c-e} *iii*) SOCl_2 , PPh_3 , $80\text{-}130^\circ\text{C}$, 7 h;^{31a} *iv*) $\text{Na}_2\text{S}\cdot 9\text{H}_2\text{O}$, S, DMF, $80\text{-}85^\circ\text{C}$, 72 h;^{31c-h} *v*) 1. NaBH_4 , Se, EtOH, reflux, 2 h; 2. DMF, 130°C , 30 min.^{31i,k,l,32}



Compound **11** tends to polymerize in the absence of a solvent as it was found for analogous 1,2-diselenolane derivatives.^{24c,33} The storage of **11** in a pentane solution prevents polymerization and enables its characterization. The ^1H NMR spectrum of **11** shows two multiplets centered at 3.34 and 3.03 ppm for the non-equivalent protons of the SeCH_2 groups. Another resonance signal for the remaining CH of the diselenolane ring is observed superimposed by the multiplet at 3.03 ppm. The protons of the CH_3 group resonate as a doublet at 1.13 ppm with a $^3J_{\text{H-H}}$ coupling constant of 6.0 Hz. Furthermore, the $^{13}\text{C}\{^1\text{H}\}$ NMR spectrum shows three signals at 46.0, 38.4 and 19.3 ppm for the CH , SeCH_2 and CH_3 groups, respectively. Caused by the proximity to the diselenide unit, the CH_2 groups exhibit ^{77}Se satellites with a $^1J_{\text{C-Se}}$ coupling constant of 65.5 Hz. In addition, the chemical shift for the two equivalent ^{77}Se atoms (277 ppm, determined by $^1\text{H}^{77}\text{Se}$ HMBC NMR) is in the typical range for the substituted 1,2-diselenolane derivatives and the $^1J_{\text{C-Se}}$ coupling constant is also comparable to those for other 1,2-diselenolanes as well as dialkyl diselenides.^{31i,34}

Synthesis and characterization of complexes 5 and 6. Treatment of $\text{Fe}_3(\text{CO})_{12}$ with the 1,2-diselenolanes **11** and **12**, respectively, in toluene at 100 °C for two hours followed by subsequent column chromatography afforded complexes **5** and **6** in 58.5 % and 62.3 % yield, respectively (Scheme 2). Complexes **5** and **6** as well as the previously reported **1-4** (Supporting Information) have been characterized by spectroscopic methods (^1H NMR, $^{13}\text{C}\{^1\text{H}\}$ NMR, $^1\text{H}^{77}\text{Se}$ HMBC NMR (for **4**) and IR), mass spectrometry, elemental analysis and X-ray crystallography for **5** and **6**.

Scheme 2. Synthesis of the [FeFe]-hydrogenase models **5** and **6**.



The ^1H NMR resonance signals for the SeCH_2 protons of **4-6** are shifted downfield by compared to their analogous S-containing complexes **1-3** whereas the resonances of the protons on the bridgehead in **4** (SeCH_2CH_2) and **5** (SeCH_2CHMe) are shifted upfield.^{24c,30f,35} Moreover, both of the SeCH_2 and the bridgehead carbon atoms (SeCH_2CR_2) in **4-6** resonate at lower frequencies in the $^{13}\text{C}\{^1\text{H}\}$ NMR spectra compared to the S-containing complexes **1-3** (see Table 1). In contrast to previous investigations, the resonance signals at 30.1 and 14.5 ppm in the $^{13}\text{C}\{^1\text{H}\}$ NMR spectrum of **4** are assigned to SeCH_2CH_2 and SeCH_2 , respectively.^{30f,24c} The resonance at 14.5 ppm clearly shows ^{77}Se satellites with a $^1J_{\text{C-Se}}$ coupling constant of 76.9 Hz indicating that the CH_2 group is bound directly to a selenium atom. This coupling constant ($^1J_{\text{C-Se}}$) is similar to those found for complexes **5** (77.6 Hz) and **6** (82.3 Hz) (Table 1), but it is larger than that in the case of the 1,2-diselenolane compounds **11** and **12**. The ^{13}C resonance signals of the SeCH_2 groups appear at higher frequencies if the protons at the bridgehead carbon atoms of the ligand $\mu\text{-(SeCH}_2)_2\text{CR}_2$ are stepwise substituted by methyl groups (14.5, 20.6 and 25.2 ppm for

complexes **4**, **5** and **6**, respectively). A similar influence of the methyl groups is also observed for the analogous S-containing complexes **1-3**.

Table 1. Characteristic $^{13}\text{C}\{^1\text{H}\}$ NMR spectroscopic data and CO stretching frequencies for complexes **1-6** (b = broad). $[\text{Fe}_2(\text{CO})_6\{\mu\text{-(XCH}_2)_2\text{CRR}'\}]$ (X = S or Se)

Complex	$\delta(\text{CO})$ [ppm]	$\delta(\text{XCH}_2)$ [ppm]	$\delta(\text{XCH}_2\text{CR}_2)$ [ppm]	$\nu(\text{CO})$ [cm^{-1}]
1	207.1	23.2	30.3	2070, 2032 (b), 1982, 1945 (b)
2	207.9	30.1	38.1	2079, 2070 (b), 2024 (b), 1992 (b), 1980,
	207.6			1956 (b)
3	207.7	33.4	33.4	2077, 2068, 2020 (b), 1991 (b), 1953 (b)
4	208.7	14.5	30.1	2062, 2026 (b), 1976 (b), 1942 (b)
		$^1J_{\text{C-Se}} = 76.9$ Hz		
5	209.0	20.6	37.3	2072, 2060 (b), 2015 (b), 1984 (b), 1973,
	208.6	$^1J_{\text{C-Se}} = 77.6$ Hz		1948 (b)
6	208.6	25.0	32.9	2071, 2060, 2056, 2014, 1980, 1950 (b)
		$^1J_{\text{C-Se}} = 82.3$ Hz		

As shown in Table 1 only one signal for the carbonyl ligands is detected in the $^{13}\text{C}\{^1\text{H}\}$ NMR spectra of complexes **1**, **3**, **4** and **6** whereas the less symmetric complexes **2** and **5** show two signals indicating two different $\text{Fe}(\text{CO})_3$ moieties at room temperature. This desymmetrizing effect of the ligand $\mu\text{-(SeCH}_2)_2\text{CHMe}$ was also obvious in the case of $[\text{Fe}_2(\text{CO})_6\{\mu\text{-(SCH}_2)_2(\text{Ph})\text{P=O}\}]^{28}$ and $[\text{Fe}_2(\text{CO})_6\{\mu\text{-(SCH}_2)_2\text{CHPh}\}]^{36}$. Interestingly, the replacement of one CO ligand in $[\text{Fe}_2(\text{CO})_6\{\mu\text{-(SCH}_2)_2(\text{Ph})\text{P=O}\}]^{37}$ or $[\text{Fe}_2(\text{CO})_6\{\mu\text{-(SCH}_2)_2\text{CHPh}\}]^{36}$ by PR_3 was found to occur regioselectively at one type of the $\text{Fe}(\text{CO})_3$ units. Indeed, Rauchfuss and co-workers also described the regiochemistry of substitution of one CO ligand in $[\text{Fe}_2(\text{CO})_6\{\mu\text{-(SCHMe)}_2\text{NH}\}]$ by PMe_3 or PPh_3 .³⁸ It is evident from Table 1 that the ^{13}C resonances for the CO ligands appear at higher frequencies if the sulfur atoms are substituted by

selenium atoms, which is related to the different electronic properties of the Fe_2X_2 units ($\text{X} = \text{S}$ or Se).^{24c,30f,35a,b} Due to the stronger donor ability of the selenium atom compared to that of the sulfur atom, the $\nu(\text{CO})$ bands in the IR spectra of **4-6** appear at smaller wavenumbers compared to those of **1-3** (see Table 1).^{24c,30f,35a,b} The resonance signals of the ^{77}Se atoms (determined by $^1\text{H}^{77}\text{Se}$ HMBC NMR spectroscopy) are quite sensitive to the substitution pattern of the bridgehead carbon atom. For complex **4**, a singlet at 143.9 ppm is observed for its two equivalent selenium atoms whereas complexes **5** and **6** show signals at 173.42 and 78.91 ppm, respectively (Figure S1 shows the ^{77}Se NMR spectra of **5** and **6**). The latter one represents a typical chemical shift that is also found in the case of the complex $[\text{Fe}_2(\text{CO})_6\{\mu-(\text{SeCH}_2)_2\text{C}(\text{CH}_2\text{OH})_2\}]$ having a disubstituted bridgehead carbon atom.²⁷

Molecular structures. Single crystals suitable for X-ray diffraction studies were obtained by slow evaporation of a saturated solution of **5** or **6** in pentane at -24°C . The molecular structures of complexes **5** and **6** are shown in Figure 4. Three crystallographically independent molecules in the unit cell of complex **6** were determined, only one of them is shown in Figure 4. Overall, the molecular structures of complexes **5** and **6** are almost identical to those reported for the corresponding sulfur derivatives **2** and **3**. As observed for complex **2**, the methyl group in **5** shows an equatorial orientation on the $\text{Fe1Se}_2\text{C}_2\text{C}_2$ six-membered ring and is orientated away from the apical CO ligand.^{30c} Because of the larger size of the selenium atom compared to the sulfur atom, a lengthening of chalcogen-containing bonds as well as the Fe-Fe-bonds are observed for **4-6** compared to **1-3**.³⁹ The Fe-Fe bond length is determined as 2.5353(7) Å for complex **5** and therefore about 0.05 Å larger than that for the sulfur derivative **2**.^{30c} As found for **2** and **5**, the Fe-Fe bond length in **6** (2.535 Å, average of the three independent molecules) is longer than that in **3** (2.494(6) Å) compared to that in the analogous S-containing complex **3**.^{30d}

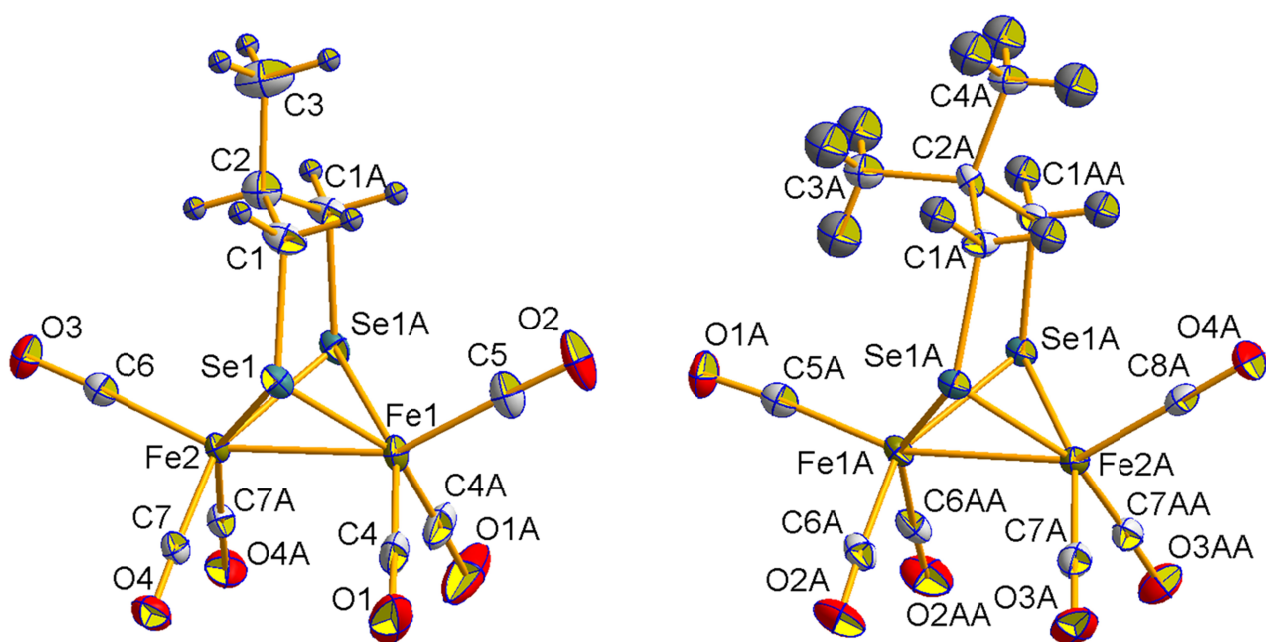


Figure 4. Molecular structures of **5** (to the left) and **6** (to the right). Thermal ellipsoids are drawn at 50 % probability level. Selected bond lengths [\AA] and angles [$^\circ$] for **5**: Fe1-Fe2 2.5353(7), Fe1-Se1 2.3811(5), Fe1-Se1A 2.3810(5), Fe2-Se1 2.3818(4), Fe2-Se1A 2.3819(4), Se1-C1 1.969(3), Se1A-C1A 1.969(3), Se1-C1-C2 117.9(2), C1-C2-C1A 115.4(4), C2-C1A-Se1A 117.9(2). Selected bond lengths [\AA] and angles [$^\circ$] for **6**: Fe1A-Fe2A 2.5273(13), Fe1A-Se1AA 2.3832(8), Fe1A-Se1A 2.3832(8), Fe2A-Se1AA 2.3835(8), Fe2A-Se1A 2.3835(8), Se1AA-C1AA 1.973(4), Se1A-C1A 1.973(4), Se1AA-C1AA-C2A 122.15(24), C1AA-C2A-C1A 111.49(22), C2A-C1A-Se1A 122.15(24).

Table 2 displays the angles $\text{Fe-Fe-C(O)}^{\text{ap}}$ (ap for apical) in complexes **4-6**. The two $\text{Fe-Fe-C(O)}^{\text{ap}}$ angles in **4** are equal reflecting a symmetrical $\text{Fe}_2(\text{CO})_6$ portion of the molecule. This symmetry is destroyed in the case of **5** and **6** for which the differences between the angles $\text{Fe-Fe-C(O)}^{\text{ap}}$ are 3.7° (for **5**) and 11.4° (for **6**). As the bulkiness of the CRR' moiety increases ongoing from **4** to **6**, the apical CO that is proximal to the CRR' moiety bends away minimizing the steric clash with CRR' while the apical CO that is distal to CRR' remains unaffected. This steric effect on the $\text{Fe-Fe-C(O)}^{\text{ap}}$ angles is also found for the analogous S-containing complexes **1-3**.^{30c-e,40} As pointed out previously by Darensbourg,^{30d,e} there is an appreciable increase in the distortion from $\text{CRR}' = \text{CH}_2$ (**1**) to CMe_2 (**3**) and the rotational

barrier of the $\text{Fe}(\text{CO})_3$ located under the bridgehead CRR' group is lower for **3** ($\text{CRR}' = \text{CMe}_2$) than that for **1**. The barrier of $\text{Fe}(\text{CO})_3$ rotation was estimated for **1** and **3** as well as various diiron dithiolato complexes by applying variable temperature $^{13}\text{C}\{^1\text{H}\}$ NMR measurements.^{30d,e} In total picture, the lower the energy barrier of $\text{Fe}(\text{CO})_3$ rotation, the easier for the complex to reach a rotated state featuring one CO in a bridging or semi-bridging position.^{30d,e} In the next section, we will discuss the impact of the steric effect on the reduction mechanism.

Table 2. Selected angles for the Se-containing complexes $[\text{Fe}_2(\text{CO})_6\{\mu-(\text{SeCH}_2)_2\text{CRR}'\}]$ (**4-6**).

Complex	R	R'	Fe-Fe-C(O) ^{ap} Angles [°] ^a
4	H	H	148.2 / 148.2
5	Me	H	151.7 / 155.4
6	Me	Me	148.5 / 159.9

^a Fe-Fe-C(O) angle for the apical carbonyl distal to the CRR' group / Fe-Fe-C angle for the apical carbonyl proximal to the CRR' group.

Electrochemistry. The electrochemistry of the models **1-4** were re-investigated to allow comparison with the new models **5** and **6** applying cyclic voltammetry and using $\text{MeCN}-[n\text{-Bu}_4\text{N}][\text{BF}_4]$ solutions. Figure 5 shows the cyclic voltammetry of complexes **1-3** and their analogous Se-containing complexes **4-6** in comparison to $[\text{Fe}_2(\text{CO})_6\{\mu\text{-bdt}\}]$ (bdt = benzenedithiolato) (**13**) that is known to be reduced with inverted potentials at scan rate $\nu = 0.2 \text{ V}\cdot\text{s}^{-1}$.²⁶ Table 3 summarizes the redox features of **1-6** and **13**. It can be noticed from Table 3 that the Se-containing complexes have less negative reduction potentials than their analogous Se-containing complexes, which is also found for other S- and Se-containing models.^{24c,30f,35a,b}

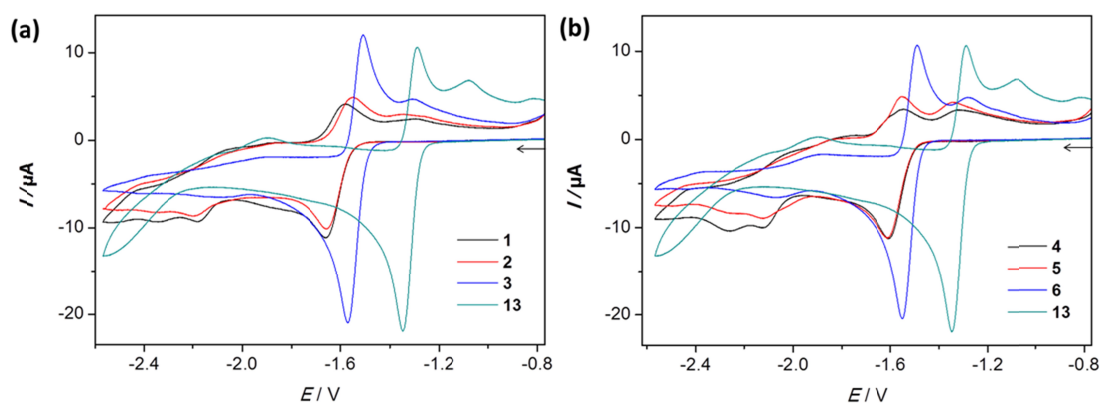


Figure 5. Cyclic voltammetry of (a) complexes **1-3** compared to **13** and (b) complexes **4-6** compared to **13** in MeCN- $[n\text{-Bu}_4\text{N}][\text{BF}_4]$ (0.1 M) solutions at $\nu = 0.2 \text{ V}\cdot\text{s}^{-1}$. The concentration of the complexes is 1.0 mM. Glassy carbon disk ($d = 1.6 \text{ mm}$). The arrows indicate the scan direction. The potentials E are given in V and referenced to the ferrocenium/ferrocene couple.

Table 3. Summary of the redox features of 1.0 mM complexes **1-6** and **13** in MeCN- $[n\text{-Bu}_4\text{N}][\text{BF}_4]$ solution measured at $\nu = 0.2 \text{ V}\cdot\text{s}^{-1}$ using glassy carbon disk ($d = 1.6 \text{ mm}$). Potentials E are given in V and referenced to the ferrocenium/ferrocene couple.

	Complex						
	1	2	3	4	5	6	13
E_{pc} [V]	-1.66	-1.66	-1.57	-1.60	-1.61	-1.55	-1.35
E_{pa} [V]	-1.58	-1.55	-1.51	-1.55	-1.55	-1.49	-1.29
$E_{1/2}$ [V] ^a	-1.62	-1.61	-1.54	-1.58	-1.58	-1.52	-1.32

^a Because the $I_{\text{pa}}/I_{\text{pc}}$ value (anodic to cathodic peak currents ratio) at $0.2 \text{ V}\cdot\text{s}^{-1}$ of the complexes is less than 1, especially for **1**, **2**, **4** and **5**, the $E_{1/2}$ can be considered as an *approximated* values.

It is evident from Figures 5a and 5b that the heights of the reduction peaks of complexes **3** ($E_{pc} = -1.57$ V), **6** ($E_{pc} = -1.55$ V) and **13** ($E_{pc} = -1.35$ V) are identical and are almost twice the peak heights of the main reduction waves of **1**, **2**, **4** and **5**. Assuming that all of the complexes have similar diffusion coefficients ($D \approx 10^{-5} \text{ cm}^2 \cdot \text{s}^{-1}$)^{23,29b,41} and by comparing their peak heights with that of **13** that is known to undergo an overall two-electron reduction²⁶ with potential inversion, we suggest that the quasi-reversible reduction waves of complexes **3** ($E_{pc} = -1.57$ V) and **6** ($E_{pc} = -1.55$ V) are due to transfer of two electrons while the reduction waves of complexes **1** ($E_{pc} = -1.66$ V), **2** ($E_{pc} = -1.66$ V), **4** ($E_{pc} = -1.60$ V) and **5** ($E_{pc} = -1.61$ V) arise from a one-electron reduction process. The cyclic voltammetry of **1**, **2**, **4** and **5** show the presence of reduction waves at $E > -2.0$ V and reduction event $E_{pc} \approx -1.85$ V overlapping clearly with the primary reduction waves of **1** and **4** (see Figure S2 for **1**). These reduction events are attributed to follow-up reactions occurring on the monoanionic species **1**⁻, **2**⁻, **4**⁻ and **5**⁻. The identities of the decomposition products of **1**⁻ were studied in great detail, in particular by IR spectroelectrochemistry and X-ray crystallography. These studies confirmed that complex **1** is reduced in a single one-electron step producing an unstable monoanion that undergoes fast irreversible chemical reactions leading to products **P1-P4** according to Scheme S1. Similar products of follow-up reactions may also be involved in the cyclic voltammetry of **2**, **4** and **5** as these complexes exhibit similar reductive features to complex **1** (see Figure 5).

The two-electron nature of the reduction peaks of **3** and **6** can be attributed to an intervening chemical process of an ECE mechanism (E = electrochemical process, C = chemical process) as reported for **13**²⁶. This chemical process involves rotation of one Fe(CO)₃ unit to locate a CO ligand in a semi-bridging position and cleavage of one Fe-S bonds.^{26b} Such a chemical process (core reorganization) stabilizes the reduced species and hence making the second electron reduction thermodynamically favoured over the first electron reduction.²⁶ Evidence for the ECE mechanism can be obtained by studying the current function ($I_{pc} / C \cdot v^{1/2}$) of the reduction wave at various scan rates.⁴² The current function is given by equation 1:

$$I_{pc} / C \cdot v^{1/2} = (2.69 \times 10^5) \cdot A \cdot D^{1/2} \cdot n^{3/2} \quad (1)$$

Where I_{pc} is the cathodic peak current in μA , C is the bulk concentration of the complex in mM, A is the surface area of the electrode in cm^2 , $D \approx 10^{-5} \text{ cm}^2 \cdot \text{s}^{-1}$ and n is the number of electrons responsible for the reduction event. In principle, in the absence of chemical complications the current function of a reduction peak should remain constant at all scan rates because $(2.69 \times 10^5) \cdot A \cdot D^{1/2} \cdot n^{3/2}$ is constant. However, in the case of an ECE mechanism of reduction for which $n = 2$, the intervening chemical process will be prevented at fast scan rates because there is not enough time for the core reorganization (rearrangement) to take place and hence the second electron transfer will not occur.⁴² Simply stated, performing the voltammetric experiment at fast scan rates prevents the intervening chemical process and alters the cathodic mechanism from ECE to a simple E process (one-electron process). In contrast to the case of ECE mechanism, the current function of an uncomplicated one-electron reduction wave ($n = 1$) is constant at all scan rates.^{42a} Figure 6 shows the scan rate dependence of the primary reduction peaks of complexes **1-6** compared to **13**, which is known to follow ECE reduction²⁶. The current function of the reduction of complexes **3** (Figure 6a) and **6** (Figure 6b) decreases significantly toward that expected for a one-electron reduction as the scan rate increases. This behaviour is similar to that in the case of complex **13** and suggests an ECE mechanism at slow scan rates that is altered to a simple E process at the short experimental time scale. In contrast, the $I_{pc} / C \cdot v^{1/2}$ value for the reduction of **1**, **2**, **4** and **5** slightly decreases as the scan rate increases. In addition, the current function of the reduction of complexes **1**, **2**, **4** and **5** is almost half that in the case of complexes **3**, **6** and **13** at slow scan rates (e.g. 0.05 to 0.2 $\text{V} \cdot \text{s}^{-1}$), but it is slightly greater than that expected for $n = 1$. This behaviour of the current function suggests an EC_i process, where C_i is an irreversible chemical process.^{42d} The slightly greater number of transferred electrons n at slow scan rates in the case of complexes **1**, **2**, **4** and **5** could be due to reduction of decomposition products of the monoanionic species, which overlaps with the primary reduction wave (Figure S2 is for the clear case of complex **1**) and contributes to its observed current. At higher scan rates, there is less time available for the decomposition of the monoanionic species to take

place and therefore the observed current would be only due to the one-electron reduction of **1**, **2**, **4** or **5** (Figures 7, S3 and S4 for **2**, **4** and **5**, respectively. For **1** see reference 22a). The cyclic voltammetry of complex **2** (Figure 7) shows that the first reduction peak is irreversible at $0.05 \text{ V}\cdot\text{s}^{-1}$. This is because there is enough time for follow-up reactions to occur that could be similar to those described for **1**, Scheme S1. Increasing the scan rate (Figure 7) enhances the chemical reversibility and at $\nu \geq 5 \text{ V}\cdot\text{s}^{-1}$, two separate one-electron reduction steps can be seen at $E_{\text{pc}1}$ and $E_{\text{pc}2}$ for the reduction of **2** and $\mathbf{2}^-$, respectively. In addition, two anodic events assigned for the oxidation of $\mathbf{2}^-$ and $\mathbf{2}^{2-}$ at $E_{\text{pa}1}$ and $E_{\text{pa}2}$, respectively, are observed. Complexes **1**, **4** and **5** exhibit similar electrochemical behaviour to that of **2** (see Figures S2 for **4** and S3 for **5**). Scheme 3 summarizes these cathodic processes of complexes **1**, **2**, **4** and **5**.

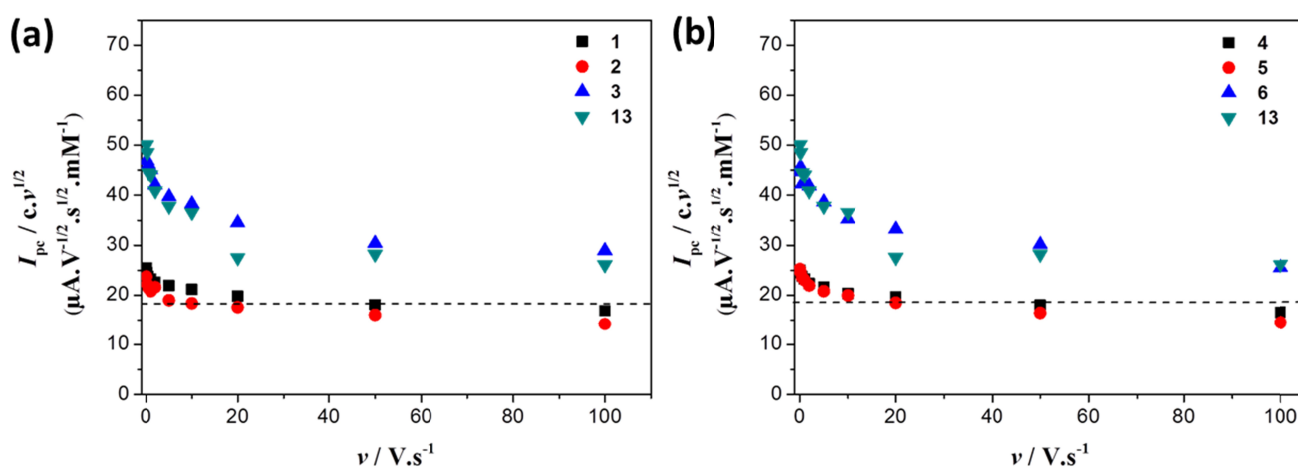


Figure 6. The scan rate dependence of the current function of the primary reduction peaks of 1.0 mM complexes (a) **1-3** compared to **13** and (b) **4-6** compared to **13**. The dashed line represents the current function expected for a one-electron process assuming $D \approx 10^{-5} \text{ cm}^2\cdot\text{s}^{-1}$.

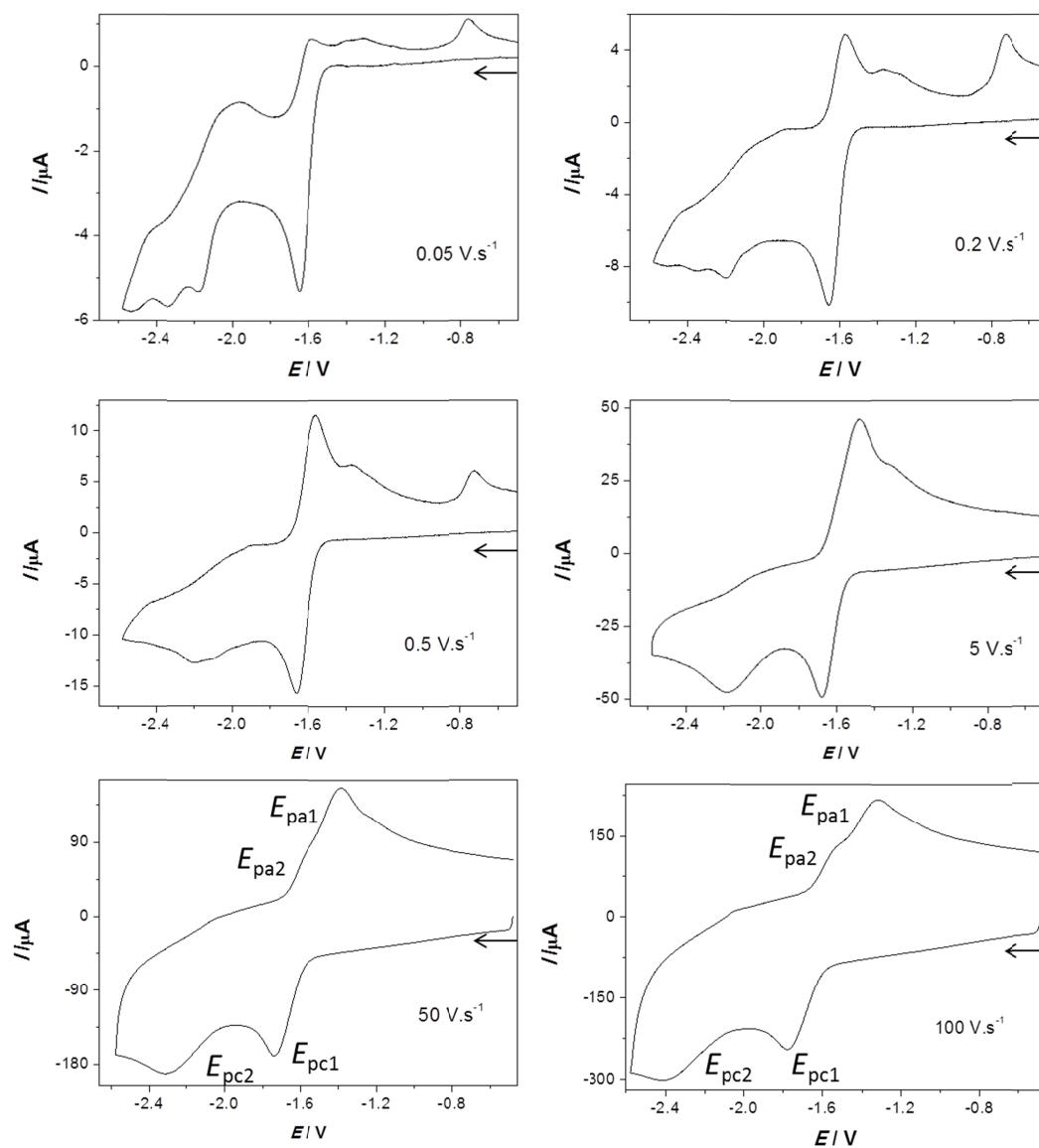
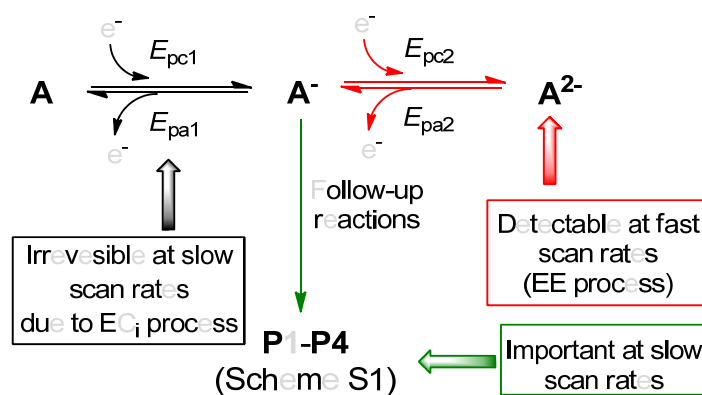


Figure 7. Cyclic voltammetry of 1.0 mM **2** in MeCN- $[n\text{-Bu}_4\text{N}][\text{BF}_4]$ (0.1 M) solution at $0.05 \text{ V}\cdot\text{s}^{-1} \leq \nu \leq 100 \text{ V}\cdot\text{s}^{-1}$. Glassy carbon disk ($d = 1.6 \text{ mm}$). The arrows indicate the scan direction. The potentials E are given in V and referenced to the ferrocenium/ferrocene couple.

Scheme 3. Cathodic processes of complexes **A** = **1**, **2**, **4** and **5** at slow and fast scan rates. For these complexes $E_{pc1} - E_{pc2} > 0$, i.e. normal ordering of potentials such that E_{pc1} is less negative than E_{pc2} .



The cyclic voltammetry of complexes **3** and **6** shows the occurrence of small irreversible reduction events near -2.08 V (Figure 5), which are attributed to reduction of daughter products of follow-up reactions involving loss of CO either from the anion or the dianion as it was found for various diiron carbonyl complexes.^{22a,29,40,43} These small reduction events disappear upon increasing the scan rate to $100 \text{ V}\cdot\text{s}^{-1}$ (Figure 8). By increasing the scan rate up to $100 \text{ V}\cdot\text{s}^{-1}$, wave-splitting is not observed for the primary reduction of complexes **3** and **6**, which implies that the second heterogeneous rate constant ks_2 of the reduction of the monoanion is larger than, or similar to ks_1 of the reduction of the neutral species **3** or **6**.^{22a,24a,26d} While in the case of complexes **1**, **2**, **4** and **5** the two overlapping re-oxidation peaks are observed at high scan rates and are attributed to the successive oxidation of the dianionic and the monoanionic species, the re-oxidation waves of **3** ($E_{pa} = -1.51 \text{ V}$ at $0.2 \text{ V}\cdot\text{s}^{-1}$) and **6** ($E_{pa} = -1.49 \text{ V}$ at $0.2 \text{ V}\cdot\text{s}^{-1}$) are not splitted at higher scan rates and are assigned to two-electron oxidation of the dianionic species regenerating the neutral complexes **3** and **6**.

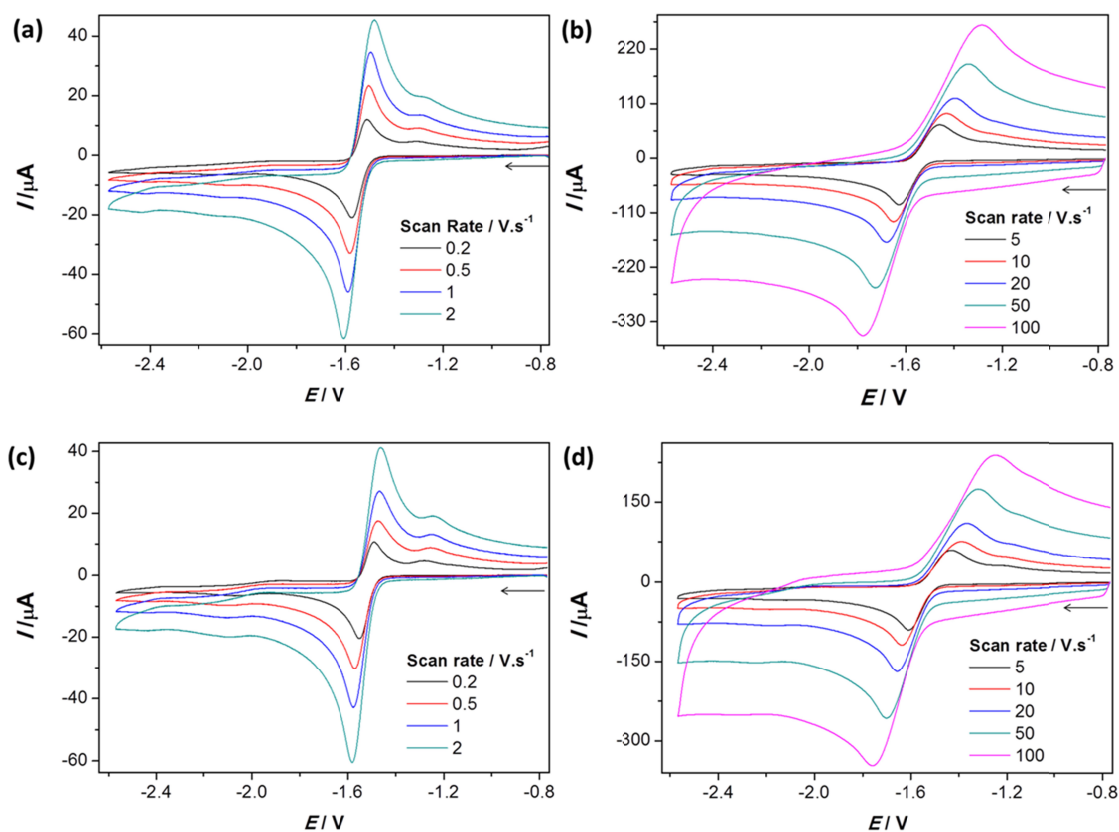
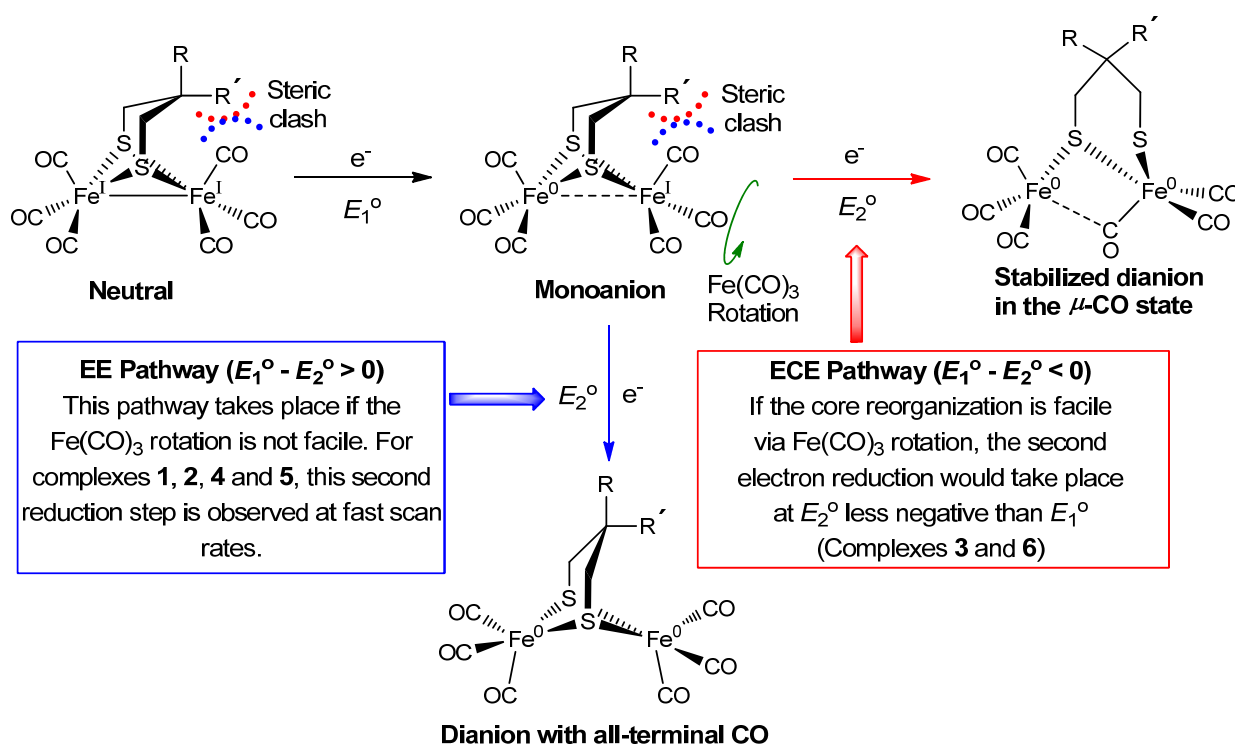


Figure 8. Cyclic voltammetry of 1.0 mM **3** (a and b) and 1.0 mM **6** (c and d) in MeCN- $[n\text{-Bu}_4\text{N}][\text{BF}_4]$ (0.1 M) solution at $0.2 \text{ V}\cdot\text{s}^{-1} \geq \nu \geq 100 \text{ V}\cdot\text{s}^{-1}$. Glassy carbon disk ($d = 1.6 \text{ mm}$). The arrows indicate the scan direction. The potentials E are given in V and referenced to the ferrocenium/ferrocene couple.

The question that arises now is: In contrast to the case of complexes **1**, **2**, **4** and **5**, *why does the cathodic mechanism of complex 3 or 6 follow an ECE pathway?* The reduction of **3** or **6** via an ECE mechanism means that the core reorganization ($\text{Fe}(\text{CO})_3$ rotation) of these complexes should be highly facile process to intervene during the electron transfer resulting in potential inversion. The bulkier CMe_2 bridgehead groups of **3** and **6** produces greater steric clash with the proximal CO ligand compared to the CH_2 bridgehead groups (in **1** and **4**) and CHMe (in **2** and **5**) as discussed before (see Table 2). The steric bulk effect of the bridgehead group on the rotational barrier of the $\text{Fe}(\text{CO})_3$ units of various diiron dithiolato complexes at the $[\text{Fe}^{\text{I}}\text{Fe}^{\text{I}}]$ redox level is revealed by Darensbourg et al. applying variable temperature $^{13}\text{C}\{^1\text{H}\}$ NMR measurements^{30d,e} and we propose that the same effect is at work in the reduced states of the complexes. Consequently, the barrier for core reorganization during the cathodic

process should be lower for **3** and **6** compared to the other complexes (**1**, **2**, **4** and **5**). Scheme 4 describes the ECE versus the simple EE reduction mechanisms of the [FeFe]-hydrogenase models. The structural changes of the reduced species in Scheme 4 are based on DFT calculations²² as well as experimental evidences²³ for the μ -CO state.

Scheme 4. Comparison between the simple EE and the ECE two-electron reduction pathways of the [FeFe]-hydrogenase models. The structures of the reduced species are based on DFT computations and experimental evidence for the μ -CO state of the dianion.



Indeed, DFT calculations showed that the most stable structure of **1**⁻ is similar to that of **1**, but with elongated Fe-Fe distance, while **1**²⁻ favours the μ -CO state rather than the structure with all-terminal CO ligands.^{22a} As discussed, the intervening core reorganization to give the μ -CO species during the cathodic process is responsible for potential inversion, which contrasts that **1** undergoes reduction in two separate steps with the normal ordering of potentials, $E_1^\circ - E_2^\circ > 0$. Even if **1**²⁻ thermodynamically favours the μ -CO state, it does not imply that an ECE mechanism of reduction should take place. It is indeed a question of kinetics of the formation of the μ -CO state and for a reduction to follow the ECE

pathway (Scheme 4), the core reorganization leading to the thermodynamically favourable μ -CO species must be facile to occur within the time scale of the voltammetry. While we describe herein the impact of the steric factor on the reduction of the [FeFe]-hydrogenase models (specifically the series **1-6**), other factors (electronic) may also play role in determining the reduction mechanism in the case of the models $[\text{Fe}_2(\text{CO})_6\{\mu\text{-(XCH}_2)_2\text{E}\}]$ (X = S or Se, E = S or Se).^{24d}

Our current electrochemical studies of the new models **5** and **6** as well as the herein re-investigations of the cyclic voltammetry of the models **1-4** reinstates the question of our previous report concerning the influence of the OH groups toward the reduction of $[\text{Fe}_2(\text{CO})_6\{\mu\text{-(XCH}_2)_2\text{C(CH}_2\text{OH)}_2\}]$ (X = S or Se)²⁷. In that report²⁷ we proposed that the replacement of the Me groups in **3** by CH₂OH groups in $[\text{Fe}_2(\text{CO})_6\{\mu\text{-(XCH}_2)_2\text{C(CH}_2\text{OH)}_2\}]$ alters the reduction mechanism from simple EE for **3** into ECE for $[\text{Fe}_2(\text{CO})_6\{\mu\text{-(XCH}_2)_2\text{C(CH}_2\text{OH)}_2\}]$, which was based on the previously reported cyclic voltammetry of **3**, where the primary reduction wave of **3** was assigned to a one-electron reduction rather than two-electron reduction as we confirmed in this report. Therefore, the ECE mechanism of reduction of $[\text{Fe}_2(\text{CO})_6\{\mu\text{-(XCH}_2)_2\text{C(CH}_2\text{OH)}_2\}]$ should also be a result of the steric effect of the two CH₂OH groups in a similar manner shown in Scheme 4, but not due to the effect of the OH \cdots S or OH \cdots Fe interactions. Our DFT computations reveal the influence of an internal interaction between the OH groups and the μ -X atom in the dianionic species.⁴⁴ This interaction causes further stabilization of the dianionic species of $[\text{Fe}_2(\text{CO})_6\{\mu\text{-(XCH}_2)_2\text{C(CH}_2\text{OH)}_2\}]$ compared to **3**²⁻ or **6**²⁻ as apparent from the less negative reduction potentials of $[\text{Fe}_2(\text{CO})_6\{\mu\text{-(XCH}_2)_2\text{C(CH}_2\text{OH)}_2\}]$ ($E_{\text{pc}} = -1.54$ V for X = S and $E_{\text{pc}} = -1.54$ V for X = Se, measured under the same conditions of the current study {see Table 3}) compared to those of **3** and **6**. The stabilization effect of the internal interactions is also described for the models shown in Figure 2 featuring agostic bonding that stabilizes the rotated structure.^{19,20}

Electrocatalytic proton reduction. Figure 9 shows the cyclic voltammetry of complexes **1**, **2**, **4** and **5** in the presence of various equivalents of acetic acid (AcOH, $\text{p}K_{\text{a}}^{\text{MeCN}} = 22.6$)^{45a}. It is evident that complexes **1-3** exhibit a catalytic behaviour near -2.2 V (Figures 9a, 9c and 9e) whereas their analogous

Se-containing complexes **4-6** show catalysis at slightly less negative potential near -2.08 V (Figures 9b, 9d and 9f). Figure S6 shows the cyclic voltammetry of various concentrations of AcOH in [*n*-Bu₄N][BF₄] in the absence of a model catalyst. The reduction of 10 mM AcOH starts near -2.1 V and reaches a peak at -2.45 V. The peak currents of the catalytic processes (Figure 9) occur at less negative potential than the peak current due to the direct reduction of AcOH. The current due to the direct reduction of 10 mM AcOH ($E = -2.45$ V) is almost half that of the catalytic processes of all complexes, except the catalysis at -1.86 V by **3** that is close to the current of the direct reduction of 10 mM AcOH. Although it is clear that the increase in the current (Figure 9) with increasing [AcOH] is due due catalytic processes, the direct reduction of AcOH might have contribution to the catalytic currents of **1-6**. However, this contribution would be less in the case of the Se-containing complexes (**4-6**) compared to their S-containing analogous **1-3** because the overpotential for the proton reduction catalyzed by **4-6** is less than that in the case of **1-3**.

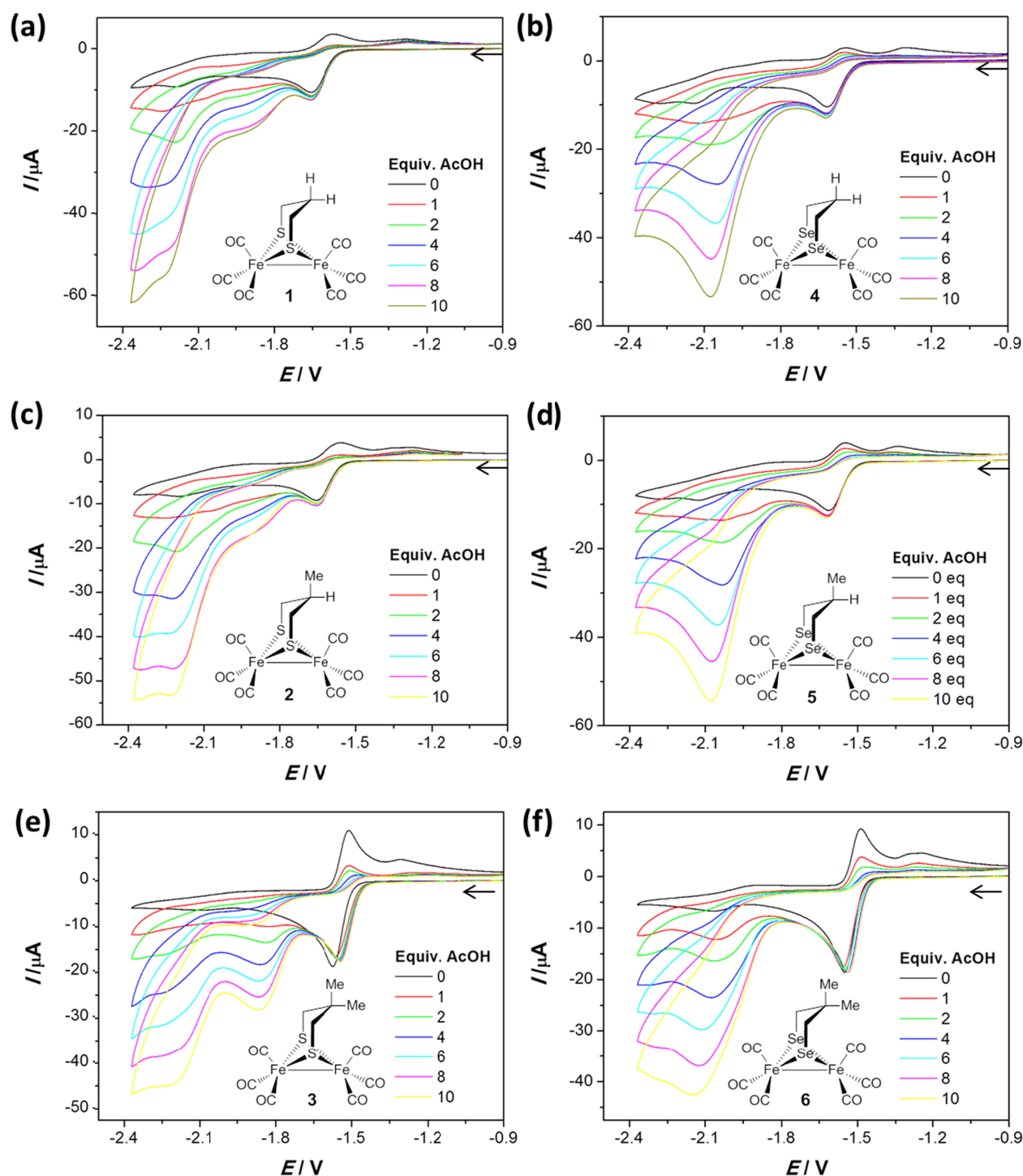


Figure 9. Cyclic voltammetry of 1.0 mM complexes 1-6 in MeCN-[*n*-Bu₄N][BF₄] (0.1 M) at 0.2 V·s⁻¹ in the presence of 1-10 equiv. AcOH. The structures of the complexes are shown as insets. Glassy carbon disk ($d = 1.6$ mm). The arrows indicate the scan direction. The potentials E are given in V and referenced to the ferrocenium/ferrocene couple.

Proton reduction cycle. We have demonstrated that the reduction of complexes **1**, **2**, **4** and **5** to give the monoanion is followed by fast decomposition at slow scan rates (Scheme 3). It has been shown by Hall et al. that the monoanion of structurally related hexacarbonyl complexes cannot be protonated at the iron core by AcOH while the dianionic species are basic enough to accept protons from AcOH to form the hydride species.⁴⁶ Darensbourg et al. also reported that the hexacarbonyl systems $[\text{Fe}_2(\text{CO})_6\{\mu\text{-(SCH}_2)_2\text{E}\}]$ do not catalyze the reduction of AcOH at the $\text{Fe}^0\text{Fe}^{\text{I}}$ level, but at the Fe^0Fe^0 state.^{29d} Thus, AcOH is unable to trap the monoanionic species of **1**, **2**, **4** and **5** from the decomposition pathways, which means that their catalytic processes shown in Figure 9 arise most likely from the products of the follow-up reactions of the monoanions. Only strong acids such as toluenesulfonic acid (HOTs, $\text{p}K_{\text{a}}^{\text{MeCN}} = 8.7$)^{45b} are able to fast protonate the monoanion $\mathbf{1}^-$ as reported by Pickett and Best et al..^{29b} In comparison, a single step two-electron reduction of **3** or **6** should be followed by protonation of the dianionic species $\mathbf{3}^{2-}$ or $\mathbf{6}^{2-}$ to afford $\mathbf{3H}^-$ or $\mathbf{6H}^-$ as was reported in the case of $\mathbf{13}^{22c}$. An experimental evidence for the protonation of the dianions $\mathbf{3}^{2-}$ or $\mathbf{6}^{2-}$ is shown in Figures 10 and S4, respectively. The disappearance of the reoxidation peak at a potential of $E_{\text{pa}} = -1.51$ V upon addition of 1 equiv. AcOH (Figure 10) suggests the protonation of $\mathbf{3}^{2-}$. Similarly, the reoxidation wave ($E_{\text{pa}} = -1.49$ V) of **6** disappears in the presence of AcOH due to protonation of $\mathbf{6}^{2-}$ (Figure S5). In the presence of various equivalents of AcOH, the current of the cathodic waves of **3** ($E_{\text{pc}} = -1.57$ V, Figure 9e) and **6** ($E_{\text{pc}} = -1.55$ V, Figure 9f) remain unaffected, but the peaks show small anodic shifts of 30 mV and 15 mV, respectively, which is typical due to protonation of the dianionic species.^{22c,47} In the case of complex **3**, two catalytic processes at -1.83 V (process I) and ca. -2.2 V (process II) are well recognized (Figure 9e) while only one catalytic process near -2.1 V can be seen in the case of complex **6** (Figure 9f). In the presence 1 equiv. AcOH in the solution of **6**, the wave observed at -2.1 V exhibit a shoulder ($E \approx -1.91$ V) and only one wave is observed at higher acid concentration (Figure S7). Processes I and II of complex **3** start in the presence of 1 and 2 equiv. AcOH, respectively. Therefore, process I may be initiated by reduction of the protonated dianion $\mathbf{3H}^-$ to give $\mathbf{3H}^{2-}$ that subsequently undergoes protonation affording the dihydrogen releasing species $\mathbf{3H}_2^-$ according to Scheme 5 (black arrows).

Based on the computational studies by Hall et al. of the possible mechanisms for the electrocatalytic proton reduction to generate H₂ by analogous models using weak and strong acids,⁴⁶ we rule out a mechanism involving protonation of **3H**⁻ by the weak acid AcOH (dashed arrows of Scheme 5) but stronger acids such as toluenesulfonic acid (HOTs, $pK_a^{\text{MeCN}} = 8.7$)^{45b} can protonate **3H**⁻ (green arrow of Scheme 5). Indeed, Glass et al. proposed a mechanism for proton reduction cycle catalyzed by complex **13** similar to that shown in Scheme 5 (black arrows).^{22c} A probable mechanism for the catalytic proton reduction via process II may start with the reduction of **3H**₂⁻ to afford **3H**₂²⁻ that releases H₂ faster than **3H**₂⁻ (see the pathway with grey arrows in Scheme 5). The analogous Se-containing complex **6** may also catalyze the reduction of protons via reaction pathways similar to those proposed for complex **3**.

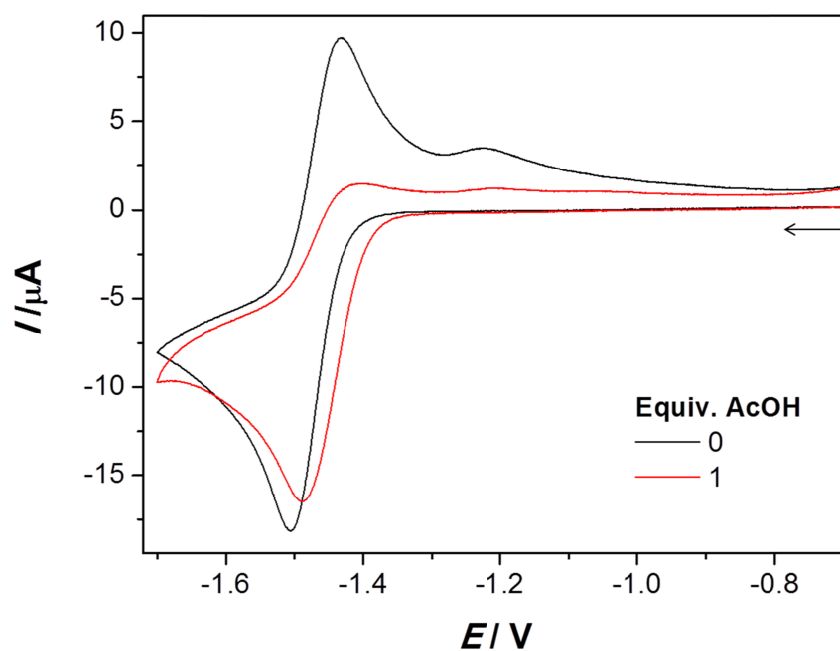
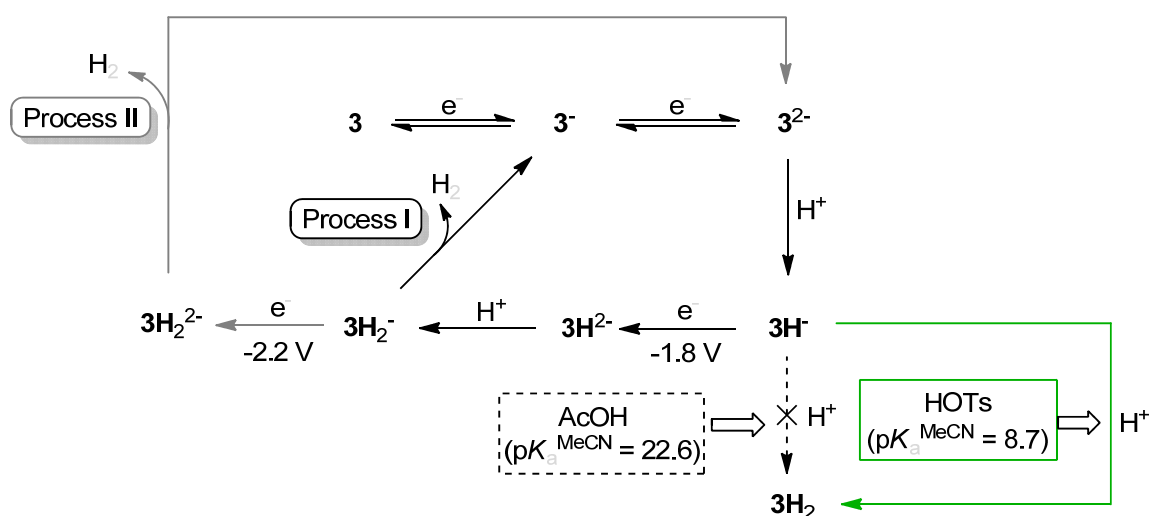


Figure 10. Cyclic voltammetry of 1.0 mM **4** in MeCN-[*n*-Bu₄N][BF₄] (0.1 M) solution at 0.2 V·s⁻¹ in the absence and presence of 1 equiv. AcOH. Glassy carbon disk (*d* = 1.6 mm). The arrow indicates the scan direction. The potentials *E* are given in V and referenced to the ferrocenium/ferrocene couple.

Scheme 5. Possible mechanism for the proton reduction cycle catalyzed by complex **3** in the presence of AcOH.



Conclusions

In this paper we report the synthesis of $[\text{Fe}_2(\text{CO})_6\{\mu-(\text{SeCH}_2)_2\text{CRR}'\}]$ (**5**: $\text{R} = \text{H}$, $\text{R}' = \text{Me}$ and **6**: $\text{R} = \text{R}' = \text{Me}$) and we compare the spectroscopic and electrochemical data of the series of complexes **1-6** having the general formula $[\text{Fe}_2(\text{CO})_6\{\mu-(\text{XCH}_2)_2\text{CRR}'\}]$ (**1**: $\text{R} = \text{R}' = \text{H}$, $\text{X} = \text{S}$, **2**: $\text{R} = \text{H}$, $\text{R}' = \text{Me}$, $\text{X} = \text{S}$, **3**: $\text{R} = \text{R}' = \text{Me}$, $\text{X} = \text{S}$, **4**: $\text{R} = \text{R}' = \text{H}$, $\text{X} = \text{Se}$). While complexes **1**, **3**, **4** and **6** exhibit one resonance in their $^{13}\text{C}\{^1\text{H}\}$ NMR spectra due to the CO groups, complexes **2** and **5** show two resonances for their CO groups due to the desymmetrizing effect of the ligand $\mu-(\text{XCH}_2)_2\text{CHMe}$ (**2**: $\text{X} = \text{S}$, **5**: $\text{X} = \text{Se}$), Table 1. The ^{13}C resonances for the CO ligands of **1-3** are down field shifted compared their analogous Se-containing **4-6** (Table 1). The SeCH_2 carbon resonance signals are shifted to lower frequencies compared to the case of SCH_2 moiety (Table 1). The $\nu(\text{CO})$ bands in the IR spectra of **4-6** appear at smaller wavenumbers compared to those of **1-3** (see Table 1) reflecting the stronger donor ability of the selenium atom compared to that of the sulfur atom. Nevertheless, the reduction potentials of **1-3** are more negative than their analogous Se-containing **4-6** (Table 3), which opposes the trend expected due to the better electron donor ability of Se atoms compared to S atoms.

Increasing the steric bulk on the bridgehead of the moiety $\mu\text{-(XCH}_2\text{)}_2\text{CRR}'$ in the series **1-3** or **4-6** results in a greater deflection of the apical CO ligand that is proximal to the CRR' group (Table 2). We have found that the steric bulk of the ligand $\mu\text{-(XCH}_2\text{)}_2\text{CRR}'$ affects the reduction mechanism of the diiron core of the complexes. It is demonstrated that only the CMe₂-containing complexes **3** and **6** follow an ECE reduction mechanism at slow scan rates of the cyclic voltammetry, which results in two-electron reduction at the same potential, while the other complexes (**1**, **2**, **4** and **5**) undergo one-electron reduction followed by decomposition of their monoanionic species at slow scan rates (EC_i, Scheme 3). The ECE reduction of **3** and **6** is demonstrated by studying their current function at various scan rates, which decreases toward that expected for one-electron reduction at high scan rates (Figure 6). The current function of **1**, **2**, **4** and **5** is closer to that expected for one-electron reduction (Figure 6). We attributed the occurrence of ECE reduction for **3** and **6** to the steric bulk effect of the bridgehead. The higher steric bulk of the CMe₂ in **3** and **6** compared to the CH₂ (in **1** and **4**) and CHMe (in **2** and **5**) results in lower Fe(CO)₃ rotational barrier and hence stabilization of the reduced species via formation $\mu\text{-CO}$ would be more facile in the case of **3** and **6**. The stabilization of the $\mu\text{-CO}$ state of the [FeFe]-hydrogenase models at the [Fe^IFe^I] redox level via the steric bulk of the bridgehead was reported by Darensbourg et al.^{30d,e}

The proton reduction catalyzed by complexes **1-6** was also investigated by cyclic voltammetry using acetic acid (AcOH) as a proton source. We propose that the decomposition products of the monoanionic species of **1**, **2**, **4** and **5** are responsible for the catalytic behaviour of the complexes because AcOH does not protonate the monoanionic species before decomposition takes place. In comparison (see Scheme 5), the ECE reduction of **3** and **6** is followed by protonation of the dianionic species to give AH^- (**A** = **3** or **6**). Further electron reduction of AH^- followed by protonation leads to release of H₂ from AH_2^- regenerating the monoanion A^- . Reduction of AH_2^- may also lead to release of H₂ from AH_2^{2-} regenerating the dianion A^{2-} . In conclusion, our studies clearly demonstrate that the reductive processes of the diiron core of the complexes as well as the catalytic proton reduction mechanisms are strongly influenced by the steric bulk of the 1,3-dichalcogenolato ligand $\mu\text{-(XCH}_2\text{)}_2\text{CRR}'$.

Experimental Section

Materials and Techniques. All reactions were performed using standard Schlenk and vacuum-line techniques under nitrogen atmosphere. The ^1H , $^{13}\text{C}\{^1\text{H}\}$, and $^1\text{H } ^{77}\text{Se}$ HMBC NMR spectra were recorded with a Bruker Avance 200 MHz, 400 MHz or 600 MHz spectrometer. Chemical shifts are given in ppm with reference to SiMe_4 (^1H , ^{13}C) or to Me_2Se ($^1\text{H } ^{77}\text{Se}$ HMBC). Mass spectra were recorded with a Finnigan MAT SSQ 710 instrument. FTIR spectra (solid state) were recorded with a Bruker Equinox 55 spectrometer equipped with an ATR unit. Elemental analysis was performed with a Leco CHNS-932 apparatus. Silica gel 60 (0.015-0.040 mm) was used for column chromatography and TLC was performed using Merck TLC aluminum sheets (Silica gel 60 F₂₅₄). Chemicals were purchased from Fisher Scientific, Aldrich or Acros and were used without further purification. All solvents were dried and distilled prior to use according to standard methods. 1,3-Diselenocyanatopropane was synthesized according to a known literature method.^{33a,48} Detailed procedures and spectroscopic data for compounds **1-4**, **7-10**, **12** and **13** are given in the supporting information.

Electrochemistry. The experiments do not involve corrections for the iR drop. Cyclic voltammetric measurements were conducted in three-electrode technique [glassy carbon disk (diameter $d = 1.6$ mm) as working electrode, Ag/Ag^+ in MeCN as reference electrode, Pt wire as counter electrode] using a Reference 600 Potentiostat (Gamry Instruments). All experiments were performed in MeCN solutions (concentration of the complexes 1.0 mM) containing 0.1 M $[n\text{-Bu}_4\text{N}][\text{BF}_4]$ at room temperature. The solutions were purged with N_2 and a stream of nitrogen was maintained over the solutions during the measurements. The vitreous carbon disk was polished on a felt tissue with alumina before each measurement. All potential values reported in this paper are referenced to the potential of the ferrocenium/ferrocene couple.

Crystal Structure Determination. The intensity data were collected on a Nonius KappaCCD diffractometer, using graphite-monochromated Mo-K_α radiation. Data were corrected for Lorentz and polarization effects; absorption was taken into account on a semi-empirical basis using multiple-

scans.⁴⁹⁻⁵¹ The structure was solved by direct methods (SHELXS)⁵² and refined by full-matrix least squares techniques against F_o^2 (SHELXL-97)⁵². All hydrogen atom positions were included at calculated positions with fixed thermal parameters.

Crystal Data for 5 : $C_{10}H_8Fe_2O_6Se_2$, $M_r = 493.78 \text{ g}\cdot\text{mol}^{-1}$, red-brown prism, size $0.048 \times 0.042 \times 0.034 \text{ mm}^3$, orthorhombic, space group $Pnma$, $a = 8.8367(2)$, $b = 9.9431(2)$, $c = 17.1843(4) \text{ \AA}$, $V = 1509.88(6) \text{ \AA}^3$, $T = -140 \text{ }^\circ\text{C}$, $Z = 4$, $\rho_{\text{calcd.}} = 2.172 \text{ g}\cdot\text{cm}^{-3}$, $\mu (\text{Mo-K}\alpha) = 67.59 \text{ cm}^{-1}$, multi-scan, transmin: 0.5107, transmax: 0.7456, $F(000) = 944$, 10608 reflections in $h(-11/10)$, $k(-12/12)$, $l(-22/22)$, measured in the range $2.37^\circ \leq \theta \leq 27.43^\circ$, completeness $\Theta_{\text{max}} = 99.6\%$, 1810 independent reflections, $R_{\text{int}} = 0.0329$, 1744 reflections with $F_o > 4\sigma(F_o)$, 103 parameters, 0 restraints, $R^1_{\text{obs}} = 0.0249$, $wR^2_{\text{obs}} = 0.0614$, $R^1_{\text{all}} = 0.0261$, $wR^2_{\text{all}} = 0.0622$, GOOF = 1.085, extrema of the final difference Fourier synthesis: 1.776 / -0.670 $e \text{ \AA}^{-3}$.

Crystal Data for 6 : $C_{11}H_{10}Fe_2O_6Se_2$, $M_r = 507.81 \text{ g}\cdot\text{mol}^{-1}$, brown prism, size $0.046 \times 0.036 \times 0.028 \text{ mm}^3$, orthorhombic, space group $Pnma$, $a = 9.1208(4)$, $b = 10.1728(5)$, $c = 51.123(3) \text{ \AA}$, $V = 4743.4(4) \text{ \AA}^3$, $T = -140 \text{ }^\circ\text{C}$, $Z = 12$, $\rho_{\text{calcd.}} = 2.133 \text{ g}\cdot\text{cm}^{-3}$, $\mu (\text{Mo-K}\alpha) = 64.58 \text{ cm}^{-1}$, multi-scan, transmin: 0.6252, transmax: 0.7456, $F(000) = 2928$, 10412 reflections in $h(-11/9)$, $k(-9/13)$, $l(-66/64)$, measured in the range $2.04^\circ \leq \theta \leq 27.55^\circ$, completeness $\Theta_{\text{max}} = 85.1\%$, 4469 independent reflections, $R_{\text{int}} = 0.0238$, 3967 reflections with $F_o > 4\sigma(F_o)$, 325 parameters, 0 restraints, $R^1_{\text{obs}} = 0.0365$, $wR^2_{\text{obs}} = 0.0698$, $R^1_{\text{all}} = 0.0444$, $wR^2_{\text{all}} = 0.0735$, GOOF = 1.227, extrema of the final difference Fourier synthesis: 0.830 / -0.613 $e \text{ \AA}^{-3}$.

4-Methyl-1,2-diselenolane (11). A Schlenk vessel was charged with 711 mg (9.00 mmol) powdered selenium and 243 mg (6.42 mmol) NaBH_4 . After cooling down to $0 \text{ }^\circ\text{C}$ 15 mL of ethanol (96 %) was added, the mixture was warmed to room temperature and additionally refluxed for two hours. Ethanol was removed by a stream of nitrogen at room temperature and 15 mL of DMF was added followed by 381 mg (3.00 mmol) of 1,3-dichloro-2-methylpropane (7). This mixture was stirred for 30 minutes at $130\text{-}140 \text{ }^\circ\text{C}$. After cooling down to room temperature 40 mL of water was added and the mixture was

three times extracted with hexane. The combined organic phases were washed with water, dried over Na_2SO_4 and concentrated to 2 mL under reduced pressure. Subsequent column chromatography (eluent: hexane) yielded the pure 4-methyl-1,2-diselenolane (**11**). This compound was stored in pentane solution to prevent polymerization. Yield: 300 mg (1.40 mmole, 46.7 %). ^1H NMR (400 MHz, CDCl_3 , 24 °C): $\delta = 3.29\text{-}3.38$ (m, 2H, SeCH_2), 2.99-3.07 (m, 3H, SeCH_2 and CH), 1.13 (d, $^3J_{\text{H-H}} = 6.0$ Hz, 3H, CH_3). $^{13}\text{C}\{^1\text{H}\}$ NMR (101 MHz, CDCl_3 , 24 °C): $\delta = 45.99$ (s, CH), 38.43 (s with ^{77}Se satellites, $^1J_{\text{C-Se}} = 65.5$ Hz, SeCH_2), 19.30 (s, CH_3). $^1\text{H}^{77}\text{Se}$ HMBC NMR (400 MHz, 76 MHz, CDCl_3 , 24 °C): $\delta = 277.3$ (s, SeCH_2). DEI-MS: $m/z = 216$ $[\text{M}]^+$. Elemental analysis for $\text{C}_4\text{H}_8\text{Se}_2 \cdot 1/25 \text{C}_6\text{H}_{14}$: calculated C 23.42, H 3.97; found C 23.40, H 3.92.

General procedure for the synthesis of complexes 1-6. Equimolar amounts of $\text{Fe}_3(\text{CO})_{12}$ and the corresponding ligand are placed in a Schlenk vessel. Toluene (20 mL for 1 mmol ligand) is added and the mixture is stirred for two hours at 100 °C. After complete reaction the solvent was removed under vacuum and the residue was purified by column chromatography using hexane as eluent.

$[\text{Fe}_2(\text{CO})_6\{\mu\text{-(SeCH}_2)_2\text{CHMe}\}]$ (5**).** This compound was prepared from 103 mg (0.481 mmol) 4-methyl-1,2-diselenolane (**11**) and 242 mg (0.481 mmol) $\text{Fe}_3(\text{CO})_{12}$ according to the general procedure. Single crystals for X-ray diffraction were grown by slow evaporation of a pentane solution at -24 °C. Yield: 139 mg (0.282 mmol, 58.5 %). ^1H NMR (400 MHz, CDCl_3 , 24 °C): $\delta = 2.54\text{-}2.68$ (m, 2H, SeCH_2), 1.32-1.44 (m, 2H, SeCH_2), 1.08-1.22 (m, 1H, CH), 0.95 (d, $^3J_{\text{H-H}} = 6.4$ Hz, 3H, CH_3). $^{13}\text{C}\{^1\text{H}\}$ NMR (101 MHz, CDCl_3 , 24 °C): $\delta = 208.98$ (s, CO), 208.61 (s, CO), 37.31 (s, CH), 23.44 (s, CH_3), 20.57 (s with ^{77}Se satellites, $^1J_{\text{C-Se}} = 77.6$ Hz, SeCH_2). $^1\text{H}^{77}\text{Se}$ HMBC NMR (400 MHz, 76 MHz, CDCl_3 , 24 °C): $\delta = 173.42$ (s, SeCH_2). IR: $\nu(\text{CO}) = 2072, 2060$ (b), 2015 (b), 1984 (b), 1973, 1948 (b). DEI-MS: $m/z = 496$ $[\text{M}]^+$, 468 $[\text{M} - \text{CO}]^+$, 440 $[\text{M} - 2\text{CO}]^+$, 412 $[\text{M} - 3\text{CO}]^+$, 384 $[\text{M} - 4\text{CO}]^+$, 356 $[\text{M} - 5\text{CO}]^+$, 328 $[\text{M} - 6\text{CO}]^+$, 272 $[\text{Fe}_2\text{Se}_2]^+$. Elemental analysis for $\text{C}_{10}\text{H}_8\text{Fe}_2\text{O}_6\text{Se}_2$: calculated C 24.32, H 1.63; found C 24.64, H 1.57.

$[\text{Fe}_2(\text{CO})_6\{\mu\text{-(SeCH}_2)_2\text{CMe}_2\}]$ (6**).** This compound was prepared from 150 mg (0.658 mmol) 4,4-dimethyl-1,2-diselenolane (**12**) and 331 mg (0.658 mmol) $\text{Fe}_3(\text{CO})_{12}$ according to the general procedure.

Single crystals for X-ray diffraction were grown by slow evaporation of a pentane solution at $-24\text{ }^{\circ}\text{C}$. Yield: 208 mg (0.410 mmol, 62.3 %). ^1H NMR (400 MHz, CDCl_3 , $24\text{ }^{\circ}\text{C}$): $\delta = 2.11$ (s with ^{77}Se satellites, $^2J_{\text{H-Se}} = 17.5$ Hz, 4H, SeCH_2), 0.97 (s, 6H, CH_3). $^{13}\text{C}\{^1\text{H}\}$ NMR (101 MHz, CDCl_3 , $24\text{ }^{\circ}\text{C}$): $\delta = 208.57$ (s, CO), 32.87 (s, CCH_3), 29.13 (s, CH_3), 25.02 (s with ^{77}Se satellites, $^1J_{\text{C-Se}} = 82.3$ Hz, SeCH_2). $^1\text{H}^{77}\text{Se}$ HMBC NMR (400 MHz, 76 MHz, CDCl_3 , $24\text{ }^{\circ}\text{C}$): $\delta = 78.91$ (s, SeCH_2). IR: $\nu(\text{CO}) = 2071$; 2060; 2056; 2014 (b); 1980 (b); 1950 (b). DEI-MS: $m/z = 510$ $[\text{M}]^+$, 482 $[\text{M} - \text{CO}]^+$, 454 $[\text{M} - 2\text{CO}]^+$, 426 $[\text{M} - 3\text{CO}]^+$, 398 $[\text{M} - 4\text{CO}]^+$, 370 $[\text{M} - 5\text{CO}]^+$, 342 $[\text{M} - 6\text{CO}]^+$, 286 $[\text{Fe}_2\text{Se}_2\text{CH}_2]^+$, 272 $[\text{Fe}_2\text{Se}_2]^+$, 192 $[\text{Fe}_2\text{Se}]^+$. Elemental analysis for $\text{C}_{11}\text{H}_{10}\text{Fe}_2\text{O}_6\text{Se}_2$: calculated C 26.02, H 1.98; found C 26.18, H 1.78.

Acknowledgments. The authors thank Hassan Abul-Futouh for measuring the ^{77}Se NMR of complexes **5** and **6**. L. A. thanks the Deutscher Akademischer Austausch Dienst (DAAD) for scholarship. This work is dedicated to the occasion of the 65th birthday of Prof. Grzegorz Mloston, University of Lodz/Poland.

Supporting Information Available. Detailed synthetic procedures and spectroscopic data for compounds **1-4**, **7-10**, **12** and **13** are given in the supporting information. Figure S1 shows the ^{77}Se NMR spectra (400 MHz, 76 MHz, CDCl_3 , $24\text{ }^{\circ}\text{C}$) of complexes **5** and **6**. Figure S2 shows the cyclic voltammetry of 1.0 mM **1** in $\text{MeCN}-[n\text{-Bu}_4\text{N}][\text{BF}_4]$ (0.1 M) at $0.2\text{ V}\cdot\text{s}^{-1}$. Figure S3 and S4 show the cyclic voltammetry of 1.0 mM **4** and 1.0 mM **5** in $\text{MeCN}-[n\text{-Bu}_4\text{N}][\text{BF}_4]$ (0.1 M) at various scan rates. Figure S5 shows the cyclic voltammetry of 1.0 mM **6** in $\text{MeCN}-[n\text{-Bu}_4\text{N}][\text{BF}_4]$ (0.1 M) solution at $0.2\text{ V}\cdot\text{s}^{-1}$ in the absence and presence of 1 and 2 equiv. AcOH. Figure S6 shows the cyclic voltammetry of different concentrations of AcOH in $\text{MeCN}-[n\text{-Bu}_4\text{N}][\text{BF}_4]$ (0.1 M) at $0.2\text{ V}\cdot\text{s}^{-1}$. In Figure S7, the cyclic voltammetry ($\text{MeCN}-[n\text{-Bu}_4\text{N}][\text{BF}_4]$ (0.1 M), $0.2\text{ V}\cdot\text{s}^{-1}$) of complex **6** in the presence of 1-4 equiv. AcOH is shown. Scheme S1 summarizes the pathways of decomposition of the monoanion **1**⁻ during the voltammetric experiment. Crystallographic data deposited at the Cambridge Crystallographic Data Centre under CCDC-1038704 for **5**, and CCDC-1038705 for **6** contain the supplementary

crystallographic data excluding structure factors; this data can be obtained free of charge via www.ccdc.cam.ac.uk/conts/retrieving.html (or from the Cambridge Crystallographic Data Centre, 12, Union Road, Cambridge CB2 1EZ, UK; fax: (+44) 1223-336-033; or deposit@ccdc.cam.ac.uk).

Table of contents

The electrochemical properties of a series of [FeFe]-hydrogenase models with the general formula $[\text{Fe}_2(\text{CO})_6\{\mu\text{-(XCH}_2)_2\text{CRR}'\}]$ ($X = \text{S}$ or Se and R or $\text{R}' = \text{H}$ or Me) was investigated. We showed that by increasing the steric bulk of the $\mu\text{-(XCH}_2)_2\text{CRR}'$ moiety, the cathodic process changes from a one-electron reduction in the case of $\text{CRR}' = \text{CH}_2$ or CHMe to a single step two-electron reduction in the case of $\text{CRR}' = \text{CMe}_2$. This change in the mechanism influences the mechanism of the catalytic proton reduction.

References

- (1) P. M. Vignais, B. Billoud and J. Meyer, *FEMS Microbiol. Rev.*, 2001, **25**, 455- 501.
- (2) P. M. Vignais and B. Billoud, *Chem. Rev.*, 2007, **107**, 4206-4272.
- (3) R. K. Thauer, *Eur. J. Inorg. Chem.*, 2011, 919-921.
- (4) E. C. Hatchikian, N. Forget, V. M. Fernandez, R. Williams and R. Cammack, *Eur. J. Biochem.*, 1992, **209**, 357-365.
- (5) M. Frey, *ChemBioChem*, 2002, **3**, 153-160.
- (6) J. C. Fontecilla-Camps, A. Volbeda, C. Cavazza and Y. Nicolet, *Chem. Rev.*, 2007, **107**, 4273-4303.
- (7) W. Lubitz, E. Reijerse and M. van Gastel, *Chem. Rev.*, 2007, **107**, 4331-4365.
- (8) W. Lubitz, H. Ogata, O. Rüdiger and E. Reijerse, *Chem. Rev.*, 2014, **114**, 4081-4148.

- (9) J. C. Fontecilla-Camps, P. Amara, C. Cavazza, Y. Nicolet and A. Volbeda, *Nature*, 2009, **460**, 814-822.
- (10) J. W. Peters, W. N. Lanzilotta, B. J. Lemon and L. C. Seefeldt, *Science*, 1998, **282**, 1853-1858.
- (11) Y. Nicolet, C. Piras, P. Legrand, C. E. Hatchikian and J. C. Fontecilla-Camps, *Structure*, 1999, **7**, 13-23.
- (12) C. Tard and C. J. Pickett, *Chem. Rev.*, 2009, **109**, 2245-2274.
- (13) F. Gloaguen and T. B. Rauchfuss, *Chem. Soc. Rev.*, 2009, **38**, 100-108.
- (14) J. -F. Capon, F. Gloaguen, F. Y. Pétilion, P. Schollhammer and J. Talarmin, *Coord. Chem. Rev.*, 2009, **253**, 1476-1494.
- (15) G. A. N. Felton, C. A. Mebi, B. J. Petro, A. K. Vanucci, D. H. Evans, R. S. Glass and D. L. Lichtenberger, *J. Organomet. Chem.*, 2009, **694**, 2681-2699.
- (16) S. Tschierlei, S. Ott and R. Lomoth, *Energy Environ. Sci.*, 2011, **4**, 2340-2352.
- (17) N. Wang, M. Wang, L. Chen and L. Sun, *Dalton Trans.*, 2013, **42**, 12059-12071.
- (18) T. R. Simmons, G. Berggren, M. Bacchi, M. Fontecave and V. Artero, *Coord. Chem. Rev.*, 2014, **270-271**, 127-150.
- (19) S. Munery, J. -F. Capon, L. De Gioia, C. Elleouet, C. Greco, F. Y. Pétilion, P. Schollhammer, J. Talarmin, G. Zampella, *Chem. Eur. J.* 2013, **19**, 15458-15461.
- (20) W. Wang, T. B. Rauchfuss, C. E. Moore, A. L. Rheingold, L. De Gioia, G. Zampella, *Chem. Eur. J.* 2013, **19**, 15476-15479.
- (21) R. Goy, L. Bertini, C. Elleouet, H. Görls, G. Zampella, J. Talarmin, L. De Gioia, P. Schollhammer, U. -P. Apfel, W. Weigand, *Dalton Trans.* 2014, **44**, 1690-1699.

- (22) (a) J. -F. Capon, S. Ezzaher, F. Gloaguen, F. Y. Pétilion, P. Schollhammer, J. Talarmin, T. J. Davin, J. E. McGrady, K. W. Muir, *New J. Chem.* 2007, **31**, 2052-2064. (b) G. A. N. Felton, B. J. Petro, R. S. Glass, D. L. Lichtenberger, D. H. Evans, *J. Am. Chem. Soc.* 2009, **131**, 11290-11291. (c) G. A. N. Felton, A. K. Vannucci, J. Chen, L. T. Lockett, N. Okumura, B. J. Petro, U. I. Zakai, D. H. Evans, R. S. Glass, D. L. Lichtenberger, *J. Am. Chem. Soc.* 2007, **129**, 12521-12530.
- (23) U. -P. Apfel, D. Troegel, Y. Halpin, S. Tschierlei, U. Uhlemann, H. Görls, M. Schmitt, J. Popp, P. Dunne, M. Venkatesan, M. Coey, M. Rudolph, G. J. Vos, R. Tacke, W. Weigand, *Inorg. Chem.* 2010, **49**, 10117-10132.
- (24) (a) J. Windhager, M. Rudolph, S. Bräutigam, H. Görls, W. Weigand, *Eur. J. Inorg. Chem.* 2007, 2748-2760. (b) J. Windhager, H. Görls, H. Petzold, G. Mloston, G. Linti, W. Weigand, *Eur. J. Inorg. Chem.* 2007, 4462-4471. (c) J. Windhager, R. A. Seidel, U. -P. Apfel, H. Görls, G. Linti, W. Weigand, *Chemistry. Biodiversity.* 2008, **5**, 2023-2041. (d) M. K. Harb, T. Niksch, J. Windhager, H. Görls, R. Holze, L. T. Lockett, N. Okumura, D. H. Evans, R. S. Glass, D. L. Lichtenberger, M. El-khateeb, W. Weigand, *Organometallics*, 2009, **28**, 1039-1048. (e) M. K. Harb, J. Windhager, T. Niksch, H. Görls, T. Sakamoto, E. R. Smith, R. S. Glass, D. L. Lichtenberger, D. H. Evans, M. El-khateeb, W. Weigand, *Tetrahedron* 2012, **68**, 10592-10599.
- (25) L. -C. Song, Z. -Y. Yang, H. -Z. Bian, Y. Liu, H. -T. Wang, X. -F. Liu, Q. -M. Hu, *Organometallics* 2005, **24**, 6126-6135.
- (26) (a) F. Gloaguen, D. Morvan, J. -F. Capon, P. Schollhammer, J. Talarmin, *J. Electroanal. Chem.* 2007, **603**, 15-20. (b) G. A. N. Felton, A. K. Vannucci, J. Chen, L. T. Lockett, N. Okumura, B. J. Petro, U. I. Zakai, D. H. Evans, R. S. Glass, D. L. Lichtenberger, *J. Am. Chem. Soc.* 2007, **129**, 12521-12530. (c) L. Schwartz, P. S. Singh, L. Eriksson, R. Lomoth, S. Ott, *C. R. Chimie* 2008, **11**, 875-889. (d) J. -F. Capon, F. Gloaguen, P. Schollhammer, J. Talarmin, *J. Electroanal. Chem.*

- 2004, **566**, 241-247. (e) J. Chen, A. K. Vannucci, C. A. Mebi, N. Okumura, S. C. Borowski, M. Swenson, L. T. Lockett, D. H. Evans, R. S. Glass, D. L. Lichtenberger *Organometallics* 2010, **29**, 5330-5340.
- (27) R. Trautwein, L. R. Almazahreh, H. Görls and W. Weigand, *Z. Anorg. Allg. Chem.*, 2013, **639**, 1512-1519.
- (28) L. R. Almazahreh, U. -P. Apfel, W. Imhof, M. Rudolph, H. Görls, J. Talarmin, P. Schollhammer, M. El-khateeb, W. Weigand. *Organometallics*, 2013, **32**, 4523-4530.
- (29) (a) U. P. Apfel, Y. Halpin, H. Görls, J. G. Vos, B. Schweizer, G. Linti, W. Weigand, *Chem. Biodiversity* 2007, **4**, 2138-2148. (b) S. J. Borg, T. Behrsing, S. P. Best, M. Razavet, X. Liu, C. J. Pickett, *J. Am. Chem. Soc.* 2004, **126**, 16988-16999. (c) A. Darchen, H. Mousser, H. Patin. *Chem. Commun.* 1988, 968-970. (d) D. Chong, I. P. Georgakaki, R. Meia-Rodriguez, J. Sanabria-Chinchilla, M. P. Soriaga, M. Y. Darensbourg, *Dalton Trans.* 2003, 4158-4163.
- (30) Complex **1**: (a) A. Winter, L. Zsolnai, G. Huttner. *Chem. Ber.* 1982, **115**, 1286-1304. (b) A. Winter, L. Zsolnai, G. Huttner. *Naturforsch., B* 1982, **37**, 1430-1436. Complex **2**: (c) A. Jablonskytė, L. R. Webster, T. R. Simmons, J. A. Wright, C. J. Pickett, *J. Am. Chem. Soc.* **2014**, *136*, 13038-13044. Complex **3**: (d) M. L. Singleton, R. M. Jenkins, C. L. Klemashevich, M. Y. Darensbourg, *C. R. Chimie* 2008, **11**, 861-874. (e) D. J. Crouthers, J. A. Denny, R. D. Bethel, D. G. Munoz, M. Y. Darensbourg, *Organometallics* 2014, **33**, 4747-4755. Complex **4**: (f) L. C. Song, B. Gai, H. T. Wang, Q. M. Hu, *J. Inorg. Biochem.* 2009, **103**, 805-812. See also ref. 24c.
- (31) Compound **7**: (a) S. E. Shevchenko, N. P. Volynskii, *Petrol. Chem.* 2008, **48**, 123-128. (b) T. Rohde, O. Huttenloch, F. Osswald, K. Wissel, 2007, WO2007028761 (A1). Compound **8**: (c) E. L. Eliel, R. O. Hutchins, *J. Am. Chem. Soc.* 1969, **91**, 2703-2715. (d) E. L. Eliel, V. S. Rao, S. Smith, R. O. Hutchins, *J. Org. Chem.* 1975, **40**, 524-526. (e) E. L. Eliel, V. S. Rao, F. G. Riddell, *J. Am. Chem. Soc.* 1976, **98**, 3583-3590. Compound **9**: 31b. Compound **10**: (f) E. W.

- Abel, P. K. Mittal, K. G. Orrell, V. Sik, *J. Chem. Soc., Dalton Trans.* 1986, 961-966. (g) P. Dhar, N. Chidambaram, S. Chandrasekaran, *J. Org. Chem.* 1992, **57**, 1699-1702. (h) V. K. Aggarwal, I. W. Davies, R. Franklin, J. Maddock, M. F. Mahon, K. C. Molloy, *J. Chem. Soc., Perkin Trans. 1* 1994, 2363-2368. Compound **12**: (i) H. J. Backer, H. J. Winter, *Recl. Trav. Ch. Pays-Ba.* 1937, **56**, 691-698. (j) E. W. Abel, P. K. Mittal, K. G. Orrell, V. Sik, *J. Chem. Soc., Dalton Trans.* 1986, 961-966. (k) E. Block, E. V. Dikarev, R. S. Glass, J. Jin, B. Li, X. Li, S.-Z. Zhang, *J. Am. Chem. Soc.* 2006, **128**, 14949-14961. (l) V. P. Ananikov, K. A. Gayduk, I. P. Beletskaya, V. N. Khrustalev, M. Y. Antipin, *Eur. J. Inorg. Chem.* 2009, 1149-1161.
- (32) E. W. Abel, P. K. Mittal, K. G. Orrell and V. Sik, *J. Chem. Soc., Dalton Trans.*, 1986, 961-966.
- (33) (a) G. T. Morgan and F. H. Burstall, *J. Chem. Soc.*, 1930, 1497-1502. (c) L. Syper, J. Mlochowski, *Tetrahedron*, 1988, **44**, 6119-6130.
- (34) (a) W. McFarlane and D. S. Rycroft, *J. Chem. Soc., Chem. Commun.*, 1973, **1**, 10-11. (b) T. Niksch, H. Görls, M. Friedrich, R. Oilunkaniemi, R. Laitinen and W. Weigand, *Eur. J. Inorg. Chem.*, 2010, 74-94.
- (35) (a) S. Gao, J. Fan, S. Sun, X. Peng, X. Zhao and J. Hou, *Dalton Trans.*, 2008, 2128-2135. (b) M. K. Harb, U. -P. Apfel, J. Kübel, H. Görls, G. A. N. Felton, T. Sakamoto, D. H. Evans, R. S. Glass, D. L. Lichtenberger, M. El-khateeb, W. Weigand, *Organometallics*, 2009, **28**, 6666-6675. (c) C. Figliola, L. Male, P. N. Horton, M. B. Pitak, S. J. Coles, S. L. Horswell and R. S. Grainger, *Organometallics*, 2014, **33**, 4449-4460. (c) M. K. Harb, U. -P. Apfel, T. Sakamoto, M. El-khateeb, W. Weigand, *Eur. J. Inorg. Chem.*, 2011, 986-993. (d) M. K. Harb, *Transit. Metal Chem.*, 2014, **39**, 647-651. (e) M. K. Harb, A. Daraosheh, H. Görls, E. R. Smith, G. Joel Meyer, M. T. Swenson, T. Sakamoto, R. S. Glass, D. L. Lichtenberger, D. H. Evans, M. El-khateeb, W. Weigand, *Heteroatom Chem.*, 2014, **25**, 592-606.
- (36) C. -G. Li, Y. Zhu, X. -X. Jiao, X. -Q. Fu, *Polyhedron*, 2014, **67**, 416-421.

- (37) L. Almazahreh, W. Imhof, J. Talarmin, P. Schollhammer, H. Görls, M. Y. El-khateeb, W. Weigand, *Dalton Trans.*, 2015, **44**, 7177-7189.
- (38) J. L. Stanley, Z. M. Heiden, T. B. Rauchfuss, S. R. Wilson, L. De Gioia, G. Zampella, *Organometallics*, 2008, **27**, 119-125.
- (39) (a) A. Bondi, *J. Phys. Chem.*, 1964, **68**, 441-451. (b) S. S. Batsanov, *J. Mol. Struct. -Theochem.*, 1999, **468**, 151-159.
- (40) E. J. Lyon, I. P. Georgakaki, J. H. Reibenspies and M. Y. Darensbourg, *Angew. Chem., Int. Ed.*, 1999, **38**, 3178-3180.
- (41) M. H. Cheah, S. J. Borg, M. I. Bondin, S. P. Best, *Inorg. Chem.*, 2004, **43**, 5635-5644.
- (42) (a) J. Courtot-Coupez, M. Gubguen, J. E. Guerchais, F. Y. Pétilion, J. Talarmin, *J. Chem. Soc. Dalton Trans.*, 1986, 1923-1929. (b) R. Goy, U. -P. Apfel, C. Elleouet, D. Escudero, M. Elstner, H. Görls, J. Talarmin, P. Schollhammer, L. González, W. Weigand, *Eur. J. Inorg. Chem.* 2013, 4466-4472. (c) A. J. Bard and L. R. Faulkner, “*Electrochemical Methods-Fundamentals and Applications*”, Wiley, New York, 1980, pp. 471-533. (d) P. Zanello, “*Inorganic Electrochemistry-Theory, Practice and Application*”, The Royal Society of Chemistry, UK, 2003, pp. 67-104.
- (43) (a) E. J. Lyon, I. P. Georgakaki, J. H. Reibenspies, M. Y. Darensbourg, *J. Am. Chem. Soc.* 2001, **123**, 3268-3278. (b) X. Zhao, I. P. Georgakaki, M. L. Miller, R. Mejia-Rodriguez, C.-H. Chiang, M. Y. Darensbourg, *Inorg. Chem.* 2002, **41**, 3917-3928. (c) R. Mejia-Rodriguez, D. Chong, J. H. Reibenspies, M. P. Soriaga, M. Y. Darensbourg, *J. Am. Chem. Soc.* 2004, **126**, 12004-12014. (d) J. W. Tye, J. Lee, H. W. Wang, R. Mejia-Rodriguez, J. H. Reibenspies, M. B. Hall, M. Y. Darensbourg, *Inorg. Chem.*, 2005, **44**, 5550-5552. (e) H. Mousser, Ph. D. Thesis, University of Rennes, France, 1987. (f) F. Robin, R. Rumin, J. Talarmin, F. Y. Pétilion, K. W. Muir, *Organometallics*, 1993, **12**, 365-380.

- (44) Unpublished results. See R. Trautwein, Ph. D. Thesis, University of Jena, Germany, 2005.
- (45) (a) K. Izutsu, *Acid–Base Dissociation Constants in Dipolar Aprotic Solvents*; Blackwell Scientific Publications, Oxford, 1990, **35**. (b) G. A. N. Felton, R. S. Glass, D. L. Lichtenberger and D. H. Evans, *Inorg. Chem.*, 2006, **45**, 9181–9184.
- (46) P. Surawatanawong, J. W. Tye, M. Y. Darensbourg, Michael B. Hall, *Dalton Trans.*, 2010, **39**, 3093-3104.
- (47) S. J. Borg, S. K. Ibrahim, C. J. Pickett, S. P. Best, *C. R. Chimie*, 2008, **11**, 852-860.
- (48) M. Clarembeau, A. Cravador, W. Dumont, L. Hevesi, A. Krief, J. Lucchetti and D. Van Ende, *Tetrahedron*, 1985, 41, 4793-4812.
- (49) *COLLECT, Data Collection Software*, Nonius B. V., Netherlands, 1998.
- (50) Z. Otwinowski and W. Minor, Processing of X-Ray Diffraction Data Collected in Oscillation Mode, in *Methods in Enzymology, Vol. 276, Macromolecular Crystallography, Part A*, edited by C. W. Carter and R. M. Sweet, Academic Press, San Diego, USA, 1997, pp. 307-326.
- (51) SADABS 2.10, Bruker-AXS inc., Madison, WI, USA, 2002.
- (52) G. M. Sheldrick, *Acta Crystallogr., Sect. A: Fundam. Crystallogr.*, 2008, **64**, 112-122.